$\mathcal{L}_1$ Adaptive Flight Control System: Systematic Design and Verification and Validation of Control Metrics

Enric Xargay*, Naira Hovakimyan†
University of Illinois at Urbana-Champaign, Urbana, IL 61801

Vladimir Dobrokhodov‡, Roman B. Statnikov§, Isaac Kaminer¶
Naval Postgraduate School, Monterey, CA 93943

Chengyu Cao‖
University of Connecticut, Storrs, CT 06269

Irene M. Gregory**
NASA Langley Research Center, Hampton, VA 23681

This paper presents preliminary results of the application of the Parameter Space Investigation method for the design of the $\mathcal{L}_1$ flight control system implemented on the two turbine-powered dynamically-scaled GTM AirSTAR aircraft. In particular, the study addresses the construction of the feasible solution set and the improvement of a nominal *prototype* design, obtained using the systematic design procedures of the $\mathcal{L}_1$ adaptive control theory. On the one hand, the results in the paper demonstrate the benefits of $\mathcal{L}_1$ adaptive control as a *verifiable* robust adaptive control architecture by validating the theoretical claims in terms of robustness and performance, as well as illustrating its systematic design procedures. On the other hand, the paper confirms the suitability of the Parameter Space Investigation method for the multicriteria design optimization of a flight control system subject to desired control specifications. Also, in order to facilitate the multicriteria analysis process, this study takes advantage of the Multicriteria Optimization and Vector Identification software package, which was designed to apply the Parameter Space Investigation method to engineering problems. The results and conclusions of this paper have contributed to the improvement of the (predicted) flying qualities and the robustness margins of the *all-adaptive* $\mathcal{L}_1$-augmented GTM AirSTAR aircraft.

Nomenclature

α	angle of attack
β	angle of sideslip
p	roll rate
A_z	vertical acceleration
δ_e	elevator deflection command
α_{cmd}	angle-of-attack pilot command
α_{des}	angle-of-attack desired response
β_{des}	sideslip-angle desired response
p_{des}	roll-rate desired response

*Doctoral Student, Dept. of Aerospace Engineering, Student Member AIAA; xargay@illinois.edu.
†Professor, Dept. of Mechanical Science and Engineering, Associate Fellow AIAA; nhovakim@illinois.edu.
‡Research Assistant Professor, Dept. of Mech. & Astronautical Eng., Senior Member AIAA; vldobr@nps.edu.
§Professor, Dept. of Information Sciences; rstatnik@nps.edu
¶Professor, Dept. of Mech. & Astronautical Eng., Member AIAA; kaminer@nps.edu.
‖Assistant Professor, Dept. of Mechanical Engineering, Member AIAA; ccao@engr.uconn.edu.
**Senior Aerospace Research Engineer, Dynamic Systems and Controls Branch, MS 308, Associate Fellow AIAA; irene.m.gregory@nasa.gov.

I. Introduction

Inner-loop adaptive flight control systems are seen as an appealing technology to improve aircraft performance with reduced pilot compensation at challenging flight conditions or in the event of control surface failures and vehicle damage. Under these conditions, which are characterized by a high degree of uncertainty with respect to a nominal aircraft model, the achievable levels of performance and flying qualities (FQ) that a nonadaptive flight control system can provide might be limited. However, several challenges for verification, validation, and certification of adaptive controllers have been identified which need to be addressed to enable the transition of adaptive control technologies into safety-critical aerospace applications.[1–3] In particular, the key hurdles for certification of adaptive flight control systems are (*i*) the lack of *transient characterization* (or *predictability*) in the closed-loop response; (*ii*) the limited *analysis framework for robustness and performance guarantees* for closed-loop adaptive systems; and (*iii*) the lack of *systematic design guidelines* to solve the trade-off between adaptation, performance, and robustness. These limitations seem to be directly related to the *asymptotic* nature of the results obtained in the development of the theory of adaptive control over the years. In this sense, it is important to emphasize that, when dealing with practical applications with stringent performance and robustness specifications, features such as boundedness, ultimate boundedness, or even asymptotic convergence, are *weak* properties for nonlinear adaptive feedback systems. Much stronger guarantees are needed. On the one hand, performance requirements demand predictable and consistent response of the closed loop system, dependent upon changes in system dynamics and reference signals. On the other hand, unmodeled dynamics, latencies, disturbances, and noise require precise quantification of the robustness and the stability margins of the feedback loop. Moreover, the lack of analytical quantification of the relationship between the adaptation process, the transient response, and the robustness margins makes the design of adaptive controllers an overly challenging problem, which is being commonly resolved by either computationally expensive Monte-Carlo simulations or time-consuming trial-and-error methods following some empirical guidelines or engineering intuition.

The $\mathcal{L}_1$ adaptive control theory[4] addresses precisely these limitations by setting in place an architecture that achieves *guaranteed transient performance* and *guaranteed robustness* in the presence of fast adaptation. The key feature of $\mathcal{L}_1$ adaptive control is the decoupling of adaptation and robustness. In fact, in $\mathcal{L}_1$ adaptive control architectures, the speed of adaptation is limited only by the available hardware –computational power and high-frequency sensor noise–, while the trade-off between performance and robustness can be addressed via conventional methods from classical and robust control. Fast adaptation, which allows for compensation of the undesirable effects of rapidly varying uncertainties and significant changes in system dynamics, is critical towards achieving guaranteed transient performance without enforcing persistency of excitation, applying gain scheduling of the control parameters, or resorting to control reconfiguration or high-gain feedback. Moreover, the *systematic design procedures* of the $\mathcal{L}_1$ adaptive control theory significantly reduce the tuning effort required to achieve desired closed-loop performance, which translates into a reduction in both design cycle time and development costs. With these features, the $\mathcal{L}_1$ adaptive control architectures provide a suitable framework for development of theoretically justified tools for Verification and Validation (V&V) of feedback systems, thus creating the opportunity to close some of the principal gaps in certification of adaptive flight control systems.

In this paper, we take advantage of the systematic design guidelines of $\mathcal{L}_1$ adaptive control for the design optimization of the $\mathcal{L}_1$ flight control system implemented on the Generic Transport Model (GTM), which is part of the Airborne Subscale Transport Aircraft Research (AirSTAR) system at the NASA Langley Research Center.[5,6] In particular, the study addresses the application of the Parameter Space Investigation (PSI) method[7] for the *construction of the feasible solution set* and for the subsequent *improvement of a nominal prototype design*. The PSI method is a "(quasi-)random hitting" procedure, and it is based on the search in a multidimensional design variable space, and is usually employed for solving multicriteria nonlinear programming problems often encountered in real-life engineering optimization problems. This method is implemented in the Multicriteria Optimization and Vector Identification (MOVI) software package,[8] which provides multiple analysis and visualization tools to assist the designer in the optimization process. The results included in this study have been produced by MOVI and are based on the full nonlinear simulation of the subscale GTM AirSTAR flight test vehicle.

The paper demonstrates that the consistent application of the systematic design guidelines of $\mathcal{L}_1$ adaptive control becomes particularly beneficial for the *construction of the feasible solution set*, which is considered the most important step in the formulation and solution of any applied optimization problem. In fact, the ability to systematically adjust the control parameters in $\mathcal{L}_1$ adaptive architectures considerably simplifies

the identification of a *nominal feasible solution* from which to start the search for other feasible solutions and the subsequent extension of the feasible solution set. The availability of an initial feasible solution may narrow the design variable space over which the search for feasible solutions should be performed, and as a consequence, the number of Monte-Carlo trials required for the construction of the feasible set may be significantly reduced. Additionally, the paper also confirms the benefits of $\mathcal{L}_1$ adaptive control as a *verifiable* robust adaptive control architecture by validating some of its theoretical claims in terms of robustness and performance. Finally, the paper illustrates the suitability of the PSI method (and the MOVI software package) as a tool for formulating and solving multicriteria optimization problems for design of adaptive flight control systems.

The paper is organized as follows. The PSI method and the MOVI software package are briefly described in Section II. The design optimization of the $\mathcal{L}_1$ flight control system for the NASA AirSTAR flight test vehicle is addressed in Section III. In particular, this section provides a detailed discussion of the different steps of the optimization process, including the identification of a feasible prototype design, the construction of the feasible solution set, and the improvement of the prototype design. Finally, Section IV summarizes the key results and contains the main conclusions.

II. Parameter Space Investigation Method

Physical nature of most real-life engineering design problems involve numerous design variables and multiple design criteria to be optimized. The latter ones, in most cases, represent conflicting objectives, and quite often lead to ill-posed formulations because the nature of the design problem might not be well understood or explored. In particular, control system design is one of those problems that require tools and methods for finding an optimal design, verifying it, and exploring its stability properties in the multidimensional design variable space.

In general, however, optimal control design leads to non-convex non-smooth optimization problems, which are generally very hard to solve. In order to overcome the difficulties of the multiobjective optimization problem, different methods and tools might be used to verify (*i*) that the feasible solution set is not empty, and (*ii*) that the behavior of feasible solutions around the optimal one is smooth, therefore guaranteeing robustness of the optimal design. One of the approaches that can help to solve control design problems, by providing an explicit mapping from an n-dimensional *design variable space* to a k-dimensional *criteria space*, is the PSI method.[7] This method explicitly addresses the issues with high dimensionality of the design variable space, functional constraint space, and criteria space, and is implemented in a user-friendly and "model agnostic" software package called MOVI. This software provides the benefits of the uniform sampling[9,10] of the multidimensional design variable space by using $\mathcal{LP}_\tau$ sequences[a], addresses functional constraints, and conveniently represents the overall quality of the obtained solutions.

A. Formulation of Multicriteria Optimization Problems

We start by considering a general multicriteria optimization problem, which takes into account sets of design variable, functional, and criteria constraints. We assume that the system to be optimized depends on n design variables, $\delta_1, \ldots, \delta_n$, which specify a point $\delta = (\delta_1, \ldots, \delta_n)$ in the n-dimensional design variable space. The design variables are subject to *design variable constraints* of the form:

$$\delta_i^* \leq \delta_i \leq \delta_i^{**}\,, \qquad i = 1, \ldots, n\,.$$

The constraints δ_i^* and δ_i^{**} define a parallelepiped Π in the n-dimensional design variable space.

The *functional constraints* can be written as:

$$C_j^* \leq f_j(\delta) \leq C_j^{**}\,, \qquad j = 1, \ldots, m\,,$$

where $f_j(\delta)$ is either an implicit or an explicit function of δ, and C_j^* and C_j^{**} are the lower and the upper admissible values of the functional relationships $f_j(\delta)$. Usually, functional relations and their constraints are system requirements that the designer can successively revise in order to improve the level of operation

[a]Other uniformly distributed sequences and nets[11–14] including custom built generators can be also successfully used in the MOVI software.

of the system under consideration. Functional constraints represent norms, standards, performance and robustness control specifications, and other functional relations among the design variables and the operational constraints of the system. The solutions in Π that satisfy the functional constraints define a subset $G \subseteq \Pi$.

The operation of the system is described by the particular performance criteria $\Phi_\ell(\delta)$, $\ell = 1, \ldots, k$, which can be either continuous or discrete. All other things being equal, it is desired that these criteria are optimized. For simplicity, we assume that all criteria are to be minimized. To enable preferences in the multiple criteria space, we introduce criteria constraints in the form:

$$\Phi_\ell(\delta) \leq \Phi_\ell^{**}\,, \qquad \ell = 1, \ldots, k\,,$$

where Φ_ℓ^{**} is the worst value of $\Phi_\ell(\delta)$ acceptable for the design. These constraints are repeatedly revised during the solution process. The solutions satisfying design variable, functional, and criteria constraints define the *feasible solution set* $D \subseteq G \subseteq \Pi$.

Then, the multicriteria optimization problem is reduced to defining the feasible solution set D and identifying a set Λ such that:

$$\Phi(\Lambda) = \min_{\delta \in D} \Phi(\delta)\,,$$

where $\Phi(\delta) = (\Phi_1(\delta), \ldots, \Phi_k(\delta))$ is the criterion vector, and Λ is the *Pareto optimal set* $\Lambda \subseteq D \subseteq G \subseteq \Pi$. To solve the optimization problem, one needs to determine the *most preferable vector* of design variables δ^0 among the vectors belonging to the set Λ.

B. Application of the Parameter Space Investigation Method

The PSI method is a "random hitting" procedure based on the systematic search in the parallelepiped Π using uniformly distributed sequences (e.g. $\mathcal{LP}_\tau$ sequences[b]). The method consists of three stages:

1. *Compilation of test tables.* First, one needs to obtain N points $\delta^1, \ldots, \delta^N$ that satisfy the functional constraints. Then, all the particular criteria $\Phi_\ell(\delta^p)$ are determined for each of the points δ^p, $p = 1, \ldots, N$. For every criteria, a test table is compiled so that the values of $\Phi_\ell(\delta^1), \ldots, \Phi_\ell(\delta^N)$ are arranged in increasing order. Taken together, these k tables form a complete *test table*.

2. *Preliminary selection of criteria constraints.* By analyzing the test table, the criteria constraints Φ_ℓ^{**} are adjusted to guarantee an acceptable or desired performance level of system operation. The adjustment of the criteria constraints requires an interactive work of the designer with the test table.

3. *Construction of the Pareto optimal set.* If at least one point δ^p can be found that satisfies the criteria constraints, the set of feasible solutions D is nonempty, and the optimization problem can be solved. Assuming the set D is not empty, the Pareto optimal set can be constructed, which allows in its turn to identify the most preferable (*optimal*) solution δ^0.

For a more detailed description of the PSI method, the reader is referred to [7], which includes numerous practical examples to illustrate the application of the method.

Remark 1 *It is important to note that, for a general multicriteria optimization problem in a multivariable design variable space, the determination of a parallelepiped* Π *containing points that satisfy desired functional (and criteria) constraints is very hard. However, if a nominal solution satisfying these constraints is known a priori, then the feasible solution set is guaranteed to be nonempty, and moreover, this nominal solution can be used –together with physical insights into the system at hand– to design an initial parallelepiped* Π.

[b] $\mathcal{LP}_\tau$ sampling is based on a mechanism for generating a uniformly-distributed deterministic sequence of points in a multi-dimensional space. Besides uniformity, which has been analytically proven to be among the best known, another important feature of the $\mathcal{LP}_\tau$ sampling is that it provides a way to add more points to the specific areas of initially sampled volume while preserving the same uniformity characteristics. This mechanism mitigates the inability to uniformly sample the criteria space. The method does it by gradually expanding the feasible solution set in the direction of the improved solution. This distinguishes this method from the random normal sampling. In particular, this additional sampling is employed when a particular area or direction of the n-dimensional space needs to be explored, for example in a directional search in the multidimensional domain.

III. $\mathcal{L}_1$ Flight Control System Design for AirSTAR GTM T2

In this section, we address the design optimization of the $\mathcal{L}_1$ flight control system ($\mathcal{L}_1$ FCS) implemented on the NASA AirSTAR's current primary flight test vehicle, the GTM tail number T2. The T2 is a twin-engine jet-powered and dynamically-scaled (5.5%) civil transport aircraft, designed and instrumented to perform control law evaluation, experiment design and modeling research, in-flight failure emulation, and flight in upset conditions. The research control law developed for the NASA AirSTAR flight test vehicle has a primary objective of achieving tracking for a variety of tasks with guaranteed stability and robustness in the presence of uncertain dynamics, such as changes due to rapidly varying flight conditions during standard maneuvers, and unexpected failures. Ideally, the flight control system should provide level 1 flying qualities under nominal as well as adverse flight conditions.

The $\mathcal{L}_1$ flight control system used for this application is a three axes angle of attack (α), roll rate (p)– sideslip angle (β) *all–adaptive flight control system*, and it compensates for both *matched* as well as *unmatched* dynamic uncertainties.[15] The flight control system consists of two decoupled $\mathcal{L}_1$ controllers, one for the longitudinal channel and another one for control of the lateral-directional dynamics. On the one hand, the longitudinal $\mathcal{L}_1$ controller is implemented as a SISO controller, and uses feedback in angle of attack and pitch rate to generate an elevator control signal in order to track angle of attack reference signals; on the other hand, the lateral/directional $\mathcal{L}_1$ controller is a MIMO architecture, and uses feedback in sideslip angle, roll rate, and yaw rate to generate aileron and rudder commands in order to track sideslip-angle and roll-rate reference signals with reduced coupling. In the current $\mathcal{L}_1$ FCS, the pilot adjusts directly the thrust level using the throttle lever. The reader is referred to [16, 17] for a more detailed explanation of the $\mathcal{L}_1$ FCS implemented on the NASA AirSTAR flight test vehicle.

The main challenge for the design of the $\mathcal{L}_1$ FCS is the *optimal tuning* of the state predictor and the low-pass filters to provide desired flying qualities with satisfactory robustness margins. While the Theory of $\mathcal{L}_1$ Adaptive Control provides partial systematic design guidelines to address the trade-off between performance and robustness, the optimization of the design of the $\mathcal{L}_1$ adaptive controller is still largely open and *hard* to address. The main difficulty is the non-convex and non-smooth nature of the underlying optimization problem that involves the $\mathcal{L}_1$-norm of cascaded linear systems. Randomized algorithms have been proven to be useful in control-related non-convex optimization problems, and therefore they appear as appealing methods for the optimal design of $\mathcal{L}_1$ adaptive controllers.[4, 18]

In general, the systematic design procedures of the $\mathcal{L}_1$ adaptive control theory can be used together with conventional methods from classical and robust control to find a nominal solution –which we will refer to as the *prototype* solution– that satisfies a given initial set of control specifications. This initial set of control specifications may be a subset of the performance and robustness requirements desired for the final design, or it may be a relaxed, less-stringent version of the complete set of control specifications. The PSI method appears then as a good tool for improvement of this prototype solution and optimization of the $\mathcal{L}_1$ FCS design, while ensuring that the closed-loop system verifies the desired performance and robustness requirements. At a first stage, and taking the *prototype* solution as a reference design, the PSI method can be used to extend the set of feasible solutions in the design variable space and provide an initial direction of improvement for the design of the flight control system. Similar to the design of the prototype solution, this first step can be based on a reduced and relaxed set of criteria and constraints. At a second stage, and once we have identified a feasible solution set in the design variable space, the PSI method can be used to find an optimal design satisfying performance and robustness constraints and delivering better criteria characteristics. Finally, the last stage of the design optimization process evaluates the sensitivity of criteria to the design variables in the vicinity of the most preferable (*optimal*) solution, which is important to ensure stability of this optimal solution.

Following this approach, we next present preliminary results on the application of the PSI method and the MOVI software to the design optimization of the $\mathcal{L}_1$ FCS for the NASA GTM. For the sake of clarity in the presentation and discussion of the results, we keep the design problem within a reasonable complexity, and the design procedure is applied to the design of the longitudinal channel only. However, it is important to mention that both the PSI and the software package MOVI were specially developed to address problems with design variable and the criteria spaces of high dimensionality. In the subsequent sections, we provide a description of the performance and robustness metrics used for this study, and obtain a prototype design that achieves desired flying qualities with satisfactory robustness margins. Then, we take advantage of the PSI method and the software package MOVI to improve the prototype design.

We notice that all of the results presented in this paper are based on the full nonlinear simulation of

the two-engine-powered dynamically-scaled GTM AirSTAR system tail number T2, which was released by NASA in December 2009.

A. Design Criteria

The set of design criteria considered in this study is chosen to evaluate performance and robustness properties of the GTM aircraft augmented with the $\mathcal{L}_1$ FCS. To provide an adequate assessment of the performance characteristics and flying qualities of the $\mathcal{L}_1$ augmented-aircraft both pilot-off-the-loop and pilot-in-the-loop performance metrics are included in the design procedure. The metrics considered can thus be classified in three different categories:

(*i*) *Pilot-off-the-loop performance metrics*

(*ii*) *Robustness metrics*

(*iii*) *Flying qualities and pilot-induced-oscillation (PIO) metrics*

Because the present paper addresses only the design of the longitudinal channel of the $\mathcal{L}_1$ FCS, the set of metrics used in this study are mainly based on the (time-domain) longitudinal response of the GTM with the $\mathcal{L}_1$ FCS closing the inner-loop. In the following sections we provide a detailed description of the specific metrics used for the design improvement of the flight control system. We note that some of the metrics used in this study were also proposed in [19] for the evaluation of aircraft augmented with adaptive flight control systems.

1. Pilot-off-the-Loop Performance Metrics

This first set of metrics evaluates the pilot-off-the-loop performance of the augmented-aircraft by characterizing its response to step inputs. In particular, the pilot-off-the-loop performance metrics are based on the time-domain response of the augmented-aircraft to a step command of 3 deg held for 4 sec in angle of attack (AOA), starting from a wings-level flight condition. The metrics try to capture the deviation of the actual response of the aircraft from a given desired response –which is defined to provide satisfactory flying qualities without reaching the physical limits of the platform–, as well as different measures of control activity, load factor, and cross-coupling.

Next we provide a description of the metrics included in the study. First, however, we need to introduce some notation to facilitate the definition of these metrics. Let t_0 be the time instant at which the step command is applied, and define t_f as the final time instant considered for performance evaluation ($t_f = t_0 + 4$ seconds). With the above notations, the metrics are defined as follows:

P1. *Final deviation:* this metric captures the final deviation of the actual AOA response from the desired AOA response 4 sec after the application of the step command. This metric is set to zero if the actual response reaches the AOA reference command before the end of the 4-second step:

$$P1 \triangleq \begin{cases} |\alpha(t_f) - \alpha_{\text{des}}(t_f)| & \text{if} \quad \alpha(t) < \alpha_{\text{cmd}} \quad \forall t \in [t_0, t_f] \\ 0 & \text{otherwise} \end{cases} .$$

This metric can be used to penalize or exclude sluggish responses. In the study conducted in this paper, this metric is normalized to the amplitude of the step command (3 deg).

P2. *Maximum deviation from desired AOA response:* this metric captures the maximum deviation (in absolute value) of the actual AOA response from the desired AOA response:

$$P2 \triangleq \max_{t \in [t_0, t_f]} |\alpha(t) - \alpha_{\text{des}}(t)| .$$

This metric can be redefined in terms of normalized AOA responses.

P3. *Integral deviation from desired AOA response:* this metric is defined as the (truncated) $\mathcal{L}_2$-norm of the deviation of the actual AOA response from the desired AOA response:

$$P3 \triangleq \int_{t_0}^{t_f} |\alpha(t) - \alpha_{\text{des}}(t)| dt .$$

Similar to *P2*, this metric can be redefined in terms of normalized AOA responses.

P4. *Overshoot in AOA response:* this metric captures possible overshoots and low-damping characteristics in the AOA response:

$$P4 \triangleq \begin{cases} \max_{t\in[t_0,t_f]} |\alpha(t)| & \text{if} \quad \alpha(t) > \alpha_{\text{cmd}} \quad \text{for some } t \in [t_0, t_f] \\ \alpha_{\text{cmd}} & \text{otherwise} \end{cases} .$$

Similar to *P1*, this metric can be normalized to the amplitude of the step command (3 deg).

P5. *Maximum deviation from desired AOA rate response:* this metric captures the maximum rate deviation (in absolute value) of the actual AOA response from the desired AOA response:

$$P5 \triangleq \max_{t\in[t_0,t_f]} |\dot{\alpha}(t) - \dot{\alpha}_{\text{des}}(t)| .$$

Similar to *P2* and *P3*, this metric can be redefined in terms of normalized AOA responses.

P6. *Integral deviation from desired AOA rate response:* this metric is defined as the (truncated) $\mathcal{L}_2$-norm of the rate deviation of the actual AOA response from the desired AOA response:

$$P6 \triangleq \int_{t_0}^{t_f} |\dot{\alpha}(t) - \dot{\alpha}_{\text{des}}(t)| dt .$$

Similar to *P2*, *P3*, and *P5*, this metric can be redefined in terms of normalized AOA responses.

The metrics *P1* to *P6* provide a good first characterization of the transient response of the augmented-aircraft when compared to a given desired response. Next, we present a set of metrics that can be extracted from the same step response and complement the metrics defined above.

P7. *Maximum vertical acceleration:* Load factor (and passenger comfort) requirements can be captured by the maximum vertical acceleration during the step response:

$$P7 \triangleq \max_{t\in[t_0,t_f]} |A_z(t)| .$$

This metric can also be normalized to the amplitude of the step command (3 deg).

P8. *Control effort:* this metric is defined as the (truncated) $\mathcal{L}_2$-norm of the elevator deflection command:

$$P8 \triangleq \int_{t_0}^{t_f} |\delta_e(t)| dt .$$

Similar to *P1*, *P4*, and *P7*, this metric can be normalized to the amplitude of the step command (3 deg). This metric can be used to penalize flight control designs that require a high control activity to achieve a desired control objective. It is important to note, however, that a high control effort might just be the result of a faster AOA response, and therefore a large *P8* might not always be an undesirable response characteristic.

P9. *Maximum elevator rate:* Excessive control rate can be identified by the following metric:

$$P9 \triangleq \max_{t\in[t_0,t_f]} |\dot{\delta}_e(t)| .$$

This metric, which can also be normalized to the amplitude of the step command (3 deg), can be used to penalize designs with high elevator rates in order to prevent undesirable effects from rate limiting.

P10. *Maximum elevator acceleration:* High-order derivatives of the control commands are coupled to the flexible modes of the aircraft. The following metric, based on the second derivative of the elevator command, can be used to capture excessive accelerations and oscillations in the control command that could potentially lead to unwanted structural mode-flight interactions:

$$P10 \triangleq \max_{t\in[t_0,t_f]} |\ddot{\delta}_e(t)| .$$

This metric can also be normalized to the amplitude of the step command (3 deg).

P11. *Maximum of $\mathcal{L}_1$ prediction error:* this metric captures the maximum error between the actual system state and the state of the $\mathcal{L}_1$ state predictor, usually denoted by $\tilde{x}(t)$:

$$P11 \triangleq \max_{t\in[t_0,t_f]} \|\tilde{x}(t)\|_\infty .$$

In $\mathcal{L}_1$ adaptive control architectures, the accurate estimation of system uncertainties and the performance guarantees rely on the (small) "size" of the prediction error $\tilde{x}(t)$. This metric can thus be used to monitor the correct functioning of the $\mathcal{L}_1$ adaptive controller.

P12. *Maximum deviation in cross-coupling dynamics:* this metric captures the lateral-directional coupling induced by a command in the longitudinal channel:

$$P12 \triangleq \max_{t\in[t_0,t_f]} |\delta_e(t)| \left((\beta(t) - \beta_{\text{des}}(t))^2 + (p(t) - p_{\text{des}}(t))^2 \right) .$$

We notice that this metric, which can also be normalized to the amplitude of the step command (3 deg), provides valuable information for the design of the lateral-directional FCS, rather than the longitudinal FCS. In fact, for the design of the longitudinal $\mathcal{L}_1$ FCS, this metric provides little information and it would be more convenient to analyze the coupling in the AOA response induced by a command either in roll rate or sideslip angle. The analysis of the response of the system to commands in the lateral-directional channel and the design of the lateral-directional $\mathcal{L}_1$ FCS are left (deliberately) for future work.

P13. *Integral deviation in cross-coupling dynamics:* this metric is the integral version of the previous cross-coupling metric and is defined as follows:

$$P13 \triangleq \int_{t_0}^{t_f} |\delta_e(t)| \left((\beta(t) - \beta_{\text{des}}(t))^2 + (p(t) - p_{\text{des}}(t))^2 \right) dt .$$

Similar to *P12*, this metric would be more adequate for the design of the lateral-directional flight control system, and it is included in this study only to illustrate a set of additional metrics that can be derived from the response of the augmented-aircraft to a command in the longitudinal channel.

2. Robustness Margins

In this preliminary study, the only robustness metric considered for optimization is the *time-delay margin* of the closed-loop adaptive system defined at the input of the aircraft (time delay inserted at the elevator deflection command), and it is also derived from the time-domain response of the augmented-aircraft. For a given wings-level flight condition and with the pilot off the loop, a small perturbation in the trim (initial) condition is introduced. The time-delay margin is determined as the minimum time delay that produces sustained oscillations in the AOA response as the $\mathcal{L}_1$ FCS tries to stabilize the aircraft at the given trim condition. In this paper, this robustness metric will be denoted by *R1*.

We notice that the time delay introduced in the elevator control channel is in addition to any time delay that is already modeled in the AirSTAR simulation environment, which amounts approximately to 25 msec.

3. Flying Qualities and PIO Tendencies

Finally, predictions for both flying qualities and PIO tendencies have also been included in order to complement the pilot-off-the-loop performance metrics presented in Section III.A.1. For this study, we consider the Time-Domain Neal-Smith (TDNS) flying qualities and PIO criteria, which was specifically developed for nonlinear aircraft dynamics and (non)linear flight control systems. The TDNS criterion is the counterpart in the time domain of the frequency-domain Neal-Smith criterion, and it is based on a step-tracking task with different acquisition-time requirements. For a detailed description of this criterion, the reader is referred to [20]. The reader can also find in [21] a study on the prediction of flying qualities and adverse pilot interactions in the GTM augmented with the $\mathcal{L}_1$ FCS.

In this paper, we will use four different metrics, extracted all of them from the TDNS criterion for an acquisition time of 1.5 sec, to characterize the flying qualities and PIO tendencies of the augmented-aircraft:

FQ1. *Tracking performance:* In the TDNS criterion, the root-mean-squared tracking error is used to evaluate the closed-loop performance with the pilot in the loop. A value of zero means that the pilot is able to perfectly track (with zero error) the reference command after the specified acquisition time.

FQ2. *Pilot workload:* In the TDNS criterion, the pilot workload is given by the pilot compensation phase angle (in degrees), which is derived from the optimal pilot model obtained from the criterion. A value of zero means that there is no need for either pilot lead compensation or lag compensation.

FQ3. *FQ level:* The two metrics above, *FQ1* and *FQ2*, are used to determine the predicted FQ level based on the FQ boundaries proposed in the criterion. *FQ3* is a discrete metric, and it only admits the values 1, 2, and 3, which correspond to level 1, level 2, and level 3 flying qualities respectively.

FQ4. *PIO tendency:* The TDNS criterion also provides a prediction for the susceptibility of the augmented-aircraft to PIO. This PIO-susceptibility metric is used to complement the flying qualities metrics discussed above. According to the TDNS criterion, a value above 100 implies that the augmented-aircraft is PIO-prone, whereas a value below 100 indicates a PIO-immune configuration.

The set of metrics described in this section will be used in the following sections to improve a prototype design of the longitudinal channel of the $\mathcal{L}_1$ FCS. For the first stages of the design –*prototype design* and *extension of the feasibility set*– only a subset of these metrics will be used. The full set of metrics will be used in the last stage to optimize the design of the flight control system.

B. Control Specifications

Based on the metrics defined in the previous section, the final design of the flight control system should *ideally* verify the following set of control specifications at the *reference flight condition* of 80 kt of (equivalent) airspeed and 1000 ft of altitude:

S1. Predicted level 1 flying qualities ($FQ3 = 1$)

S2. Time-delay margin greater than or equal to 80 msec ($R1 \geq 80$)

S3. Final value of the step response within 10% of the desired final value ($P1 \leq 0.1$)

In addition to this set of "rigid" control specifications, the design should also minimize the deviation of the actual AOA response from a desired response, which is defined by a second-order linear model with DC gain 1, natural frequency 5.5 $\frac{\text{rad}}{\text{sec}}$, damping ratio 0.85, and no zeros. Moreover, if possible at all given the control specifications above, the normalized maximum elevator rate should be less than or equal to 10 $\frac{\text{deg}}{\text{sec}}$/deg ($P9 \leq 10$); this is, however, a "soft" design constraint, in the sense that it can be relaxed to some extent if the feasible solution set turns out to be empty for $P9 \leq 10$.

C. Prototype Design

The Theory of $\mathcal{L}_1$ Adaptive Control provides a systematic framework for the design of adaptive controllers. First, due to the decoupling between adaptation and robustness, the adaptation rate can be selected to be as high as hardware permits. Next, the state predictor can be defined in terms of the desired response of the closed-loop system. And finally, the trade-off between performance and robustness can be resolved by determining the structure and bandwidth of the *linear* bandwidth-limited filters inserted in the control path. As a rule of thumb, by reducing the bandwidth of the filters, the time-delay margin of the system can be systematically increased at the cost of reduced performance, whereas increasing the bandwidth of the filters leads to improved performance of the adaptive closed-loop system with reduced robustness.

The design of the longitudinal $\mathcal{L}_1$ FCS is based on the linearized short-period dynamics of the GTM at the reference flight condition (80 kt, 1000 ft). Since the airplane is level 1 flying qualities at this flight condition[c], the desired dynamics of the state predictor are chosen to be close to those of the actual aircraft. For the nominal prototype design, the natural frequency of the poles of the system is reduced from 6 $\frac{\text{rad}}{\text{sec}}$ to 5.5 $\frac{\text{rad}}{\text{sec}}$, while the damping ratio is increased from 0.47 to 0.85. A first-order low-pass filter with DC gain 1

[c]This FQ rating is based on offset-landing tasks performed in the AirSTAR real-time simulator at NASA LaRC in the absence of atmospheric turbulence.

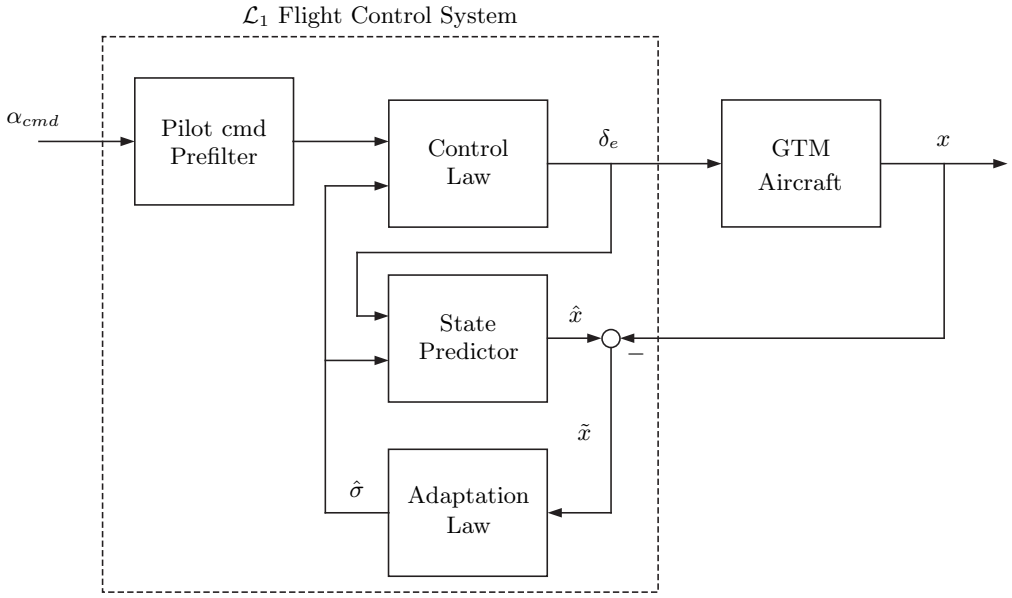

Figure 1: Block diagram of the longitudinal channel of the $\mathcal{L}_1$ flight control architecture.

and a bandwidth of 20 $\frac{\text{rad}}{\text{sec}}$ was used in the matched contribution to the elevator command, while two cascaded first-order low-pass filters were used in the unmatched channel, both having DC gain equal to 1 and bandwidths of 5 $\frac{\text{rad}}{\text{sec}}$ and 7 $\frac{\text{rad}}{\text{sec}}$ respectively. Finally, the adaptation sampling time was set to $\frac{1}{600}$ sec, which corresponds to the minimum integration step allowed in the AirSTAR flight control computer. A first-order prefilter with 20 $\frac{\text{rad}}{\text{sec}}$ of bandwidth was added to shape the pilot command. The $\mathcal{L}_1$ FCS with its main elements is represented in Figure 1. This prototype design of the state predictor, the low-pass filters, the adaptation sampling rate, and the prefilter, delivers an AOA response similar to the desired one (see Figure 2). This design also ensures a time-delay margin of the inner-loop of approximately 85 msec and a gain margin of 7.2 dB, in wings-level flight at the flight condition of 80 knots and 1000 ft. At this flight condition, the flying qualities are predicted to be level 1 and the flight control system design has no predicted PIO tendencies (for an acquisition time of 1.5 sec). Table 1 presents the values of the design variables and the corresponding set of metrics for this prototype design.

We notice that the control parameters of the $\mathcal{L}_1$ FCS –low-pass filters and adaptation rate– are used across the entire flight envelope with *no scheduling*. The reference model (state predictor), instead, is scheduled (relative to its nominal design) to provide slower pitch responses with improved performance during high-speed and high-AOA flight regimes.

D. Design Improvement

Next we present preliminary results of the application of the PSI method to the design improvement of the longitudinal channel of the $\mathcal{L}_1$ FCS. As explained earlier, the design improvement procedure consists of three steps. First, and taking the *prototype* design as a reference point, the PSI method is used to extend the feasible solution set in the design variable space, and provide an initial direction of improvement for the design of the flight control system. This first step is based on a reduced and relaxed set of criteria and constraints. Second, the PSI method is used to find an optimal design satisfying performance and robustness constraints and delivering better criteria characteristics. Finally, we conduct an analysis of the sensitivity of the criteria to the design variables in the vicinity of the optimal solution. This last step in the design optimization process is important to ensure stability of this optimal solution to small variations of the design variables.

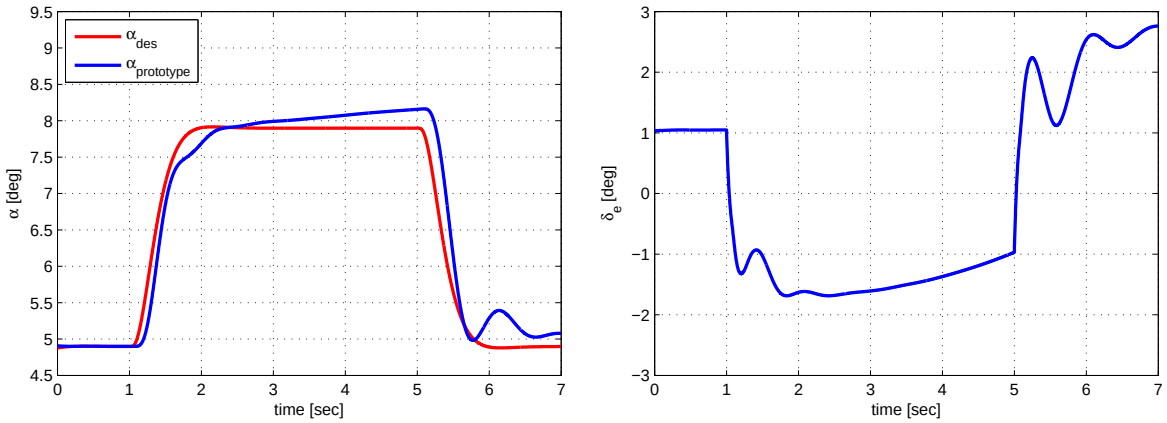

(a) Angle of attack, α (b) Elevator deflection, δ_e

Figure 2: *Prototype Design.* 3 deg-AOA step response for the prototype design.

1. *Design Variables*

We start by defining the set of parameters of the flight control architecture considered for optimization. Since the primary objective is to improve the flying qualities of the prototype design while guaranteeing satisfactory robustness margins, we include the natural frequency and the damping ratio of the poles of the state-predictor dynamics (which can speed up or slow down the response of the augmented aircraft), and the bandwidth of the low-pass filter in the matched channel (which can be used to adjust the time-delay margin of the inner-loop) as optimization parameters. In addition, we also consider the optimization of the bandwidth of the prefilter, which can be used to shape the pilot command as to prevent elevator rate limiting and avoid structural mode-flight interaction. The following list summarizes the set of optimization parameters that define the *design variable space*:

DV1. Natural frequency of the state-predictor poles

DV2. Damping ratio of the state-predictor poles

DV3. Bandwidth of the "matched" low-pass filter

DV4. Bandwidth of the pilot-command prefilter.

We notice that, consistent with the Theory of $\mathcal{L}_1$ Adaptive Control, the adaptation sampling time is set to match the minimum integration step allowed in the AirSTAR flight control computer, and therefore it is not included as an optimization parameter.

2. *Construction of the Feasible Solution Set*

The first step in the optimization of the design of the $\mathcal{L}_1$ FCS is the construction of the feasible solution set using the PSI method. For this purpose, we consider the following initial intervals of design variables, which have been defined to include the initial prototype vector (see Table 2):

$$\begin{aligned} 4 \;&\leq\; DV1 \;\leq\; 8 && \text{(rad/sec)} \\ 0.5 \;&\leq\; DV2 \;\leq\; 1.1 && \\ 5 \;&\leq\; DV3 \;\leq\; 30 && \text{(rad/sec)} \\ 10 \;&\leq\; DV4 \;\leq\; 50 && \text{(rad/sec)}\,. \end{aligned}$$

Table 1: *Prototype* design.

(a) Table of Design Variables.

Design variable	Value
DV1	$5.50 \cdot 10^{0}$
DV2	$8.50 \cdot 10^{-1}$
DV3	$2.00 \cdot 10^{1}$
DV4	$2.00 \cdot 10^{1}$

(b) Table of Criteria.

Metric	Value	Metric	Value
P1	$0.00 \cdot 10^{0}$	*P10*	$1.07 \cdot 10^{2}$
P2	$1.30 \cdot 10^{-1}$	*P11*	$7.45 \cdot 10^{-2}$
P3	$1.54 \cdot 10^{-1}$	*P12*	$1.01 \cdot 10^{-4}$
P4	$1.00 \cdot 10^{0}$	*P13*	$3.16 \cdot 10^{-5}$
P5	$3.15 \cdot 10^{-1}$	*FQ1*	$1.23 \cdot 10^{-1}$
P6	$1.49 \cdot 10^{-1}$	*FQ2*	$5.36 \cdot 10^{1}$
P7	$1.51 \cdot 10^{-1}$	*FQ3*	1
P8	$3.24 \cdot 10^{0}$	*FQ4*	$4.68 \cdot 10^{0}$
P9	$5.96 \cdot 10^{0}$	*R1*	$8.50 \cdot 10^{1}$

Table 2: Initial intervals of design variables.

Design variable	Prototype	Initial intervals of variation of design variables *(Iteration 1)*	
		min	max
DV1	$5.50 \cdot 10^{0}$	$4.00 \cdot 10^{0}$	$8.00 \cdot 10^{0}$
DV2	$8.50 \cdot 10^{-1}$	$5.00 \cdot 10^{-1}$	$1.10 \cdot 10^{0}$
DV3	$2.00 \cdot 10^{1}$	$5.00 \cdot 10^{0}$	$3.00 \cdot 10^{1}$
DV4	$2.00 \cdot 10^{1}$	$1.00 \cdot 10^{1}$	$5.00 \cdot 10^{1}$

For this first step, we consider only a subset of the control specifications described in Section III.B. In particular, the following specifications are set as "rigid" functional constraints:

$$\begin{aligned} FQ3 &\leq 1 \\ P1 &\leq 0.1 \\ P4 &\leq 1.2 \end{aligned}$$

The first and second inequalities address directly the control specifications *S1* and *S3* respectively. The third inequality imposes a 20% constraint on the overshoot in the step response, establishing thus a (loose) bound on the acceptable transient performance characteristics of the actual AOA response.

This first step is also used to find an initial direction of improvement for the design of the flight control system. More precisely, we aim here at determining tight intervals for the design variables characterizing the state predictor (*DV1* and *DV2*) that would provide level 1 flying qualities and would not deviate significantly from the desired response defined previously. To this end, the design is to be minimized with respect to the following set of *criteria*, which is a subset of the metrics described earlier in the paper:

$$P2\,, \quad P3\,, \quad P4\,, \quad P5\,, \quad P6\,, \quad FQ1\,, \quad FQ2\,.$$

The robustness metric *R1* and the PIO metric *FQ4* are not included in this first step because their evaluation is computationally expensive; these metrics will be considered in the next step of the optimization process.

Additionally, the following set of metrics is considered as *pseudocriteria*:

$$P7\,, \quad P8\,, \quad P9\,, \quad P10\,, \quad P11\,, \quad P12\,, \quad P13\,.$$

The metrics *P7* through *P10* are not included in the set of criteria to be minimized because improved flying qualities may require "high" values of these metrics. Nevertheless, including these metrics in the optimization process as pseudocriteria may provide useful information regarding the dynamics of the augmented-aircraft, and also additional performance characteristics of the set of Pareto optimal solutions. In particular, we note that the metric *P9*, which is subject to "soft" control specifications, is not specified as a functional constraint, but instead it is included as a pseudocriterion (see [7] for a detailed justification of this choice). Similarly, the metric *P11*, which can be used to monitor the correct operation of the $\mathcal{L}_1$ adaptive controller, does not need to be minimized as long as it remains a couple of orders of magnitude below the system state (truncated) $\mathcal{L}_\infty$-norm. Finally, as explained previously, the metrics *P12* and *P13* are to be considered only for the design of the lateral-directional flight control system, and therefore they are not included as criteria.

Next we present the results obtained in this first step of the optimization process, which are based on a single iteration using 1024 design variable vectors generated with uniformly distributed sequences.

Out of the 1024 samples in the design variable space, 427 vectors did not satisfy the "rigid" functional constraints. In particular, 160 design variable vectors failed the 20% overshoot functional constraint, and 267 failed the level 1 flying qualities constraint. None of the design variable vectors failed the final value functional constraint. The 427 solutions that did not satisfy the functional constraints entered the *tables of functional failures*. A careful analysis of the design variable vectors contained in this table indicates that (*i*) solutions characterized by low natural frequencies and high damping ratios of the state-predictor poles ($DV1 < 5$ and $0.95 < DV2$) fail the level 1 flying qualities functional constraint; and (*ii*) solutions with very high natural frequencies of the state-predictor poles ($7.6 < DV1$) or solutions with high natural frequencies and low damping ratios of the state-predictor poles ($7 < DV1 < 7.6$ and $DV2 < 0.6$) fail the overshoot functional constraint. The first set of design variable vectors leads to slow responses of the augmented-aircraft to pilot commands, which require moderate or considerable pilot compensation and thus result in predicted level 2 flying qualities. The second set corresponds to solutions providing fast responses to step commands with big overshoots, which differ significantly from the desired response for the augmented-aircraft.

The remaining 597 vectors which did satisfy the "rigid" functional constraints were used to construct the *test table*. While analyzing the test table, the following criteria constraints were formulated:

P2	$\leq$	0.2	(min)	*P9*	$\leq$	15	(pseudo)
P3	$\leq$	0.2	(min)	*P10*	$\leq$	300	(pseudo)
P4	$\leq$	1.05	(min)	*P11*	$\leq$	0.25	(pseudo)
P5	$\leq$	1	(min)	*P12*	$\leq$	0.01	(pseudo) .
P6	$\leq$	0.3	(min)	*P13*	$\leq$	0.01	(pseudo)
P7	$\leq$	0.25	(pseudo)	*FQ1*	$\leq$	0.1	(min)
P8	$\leq$	5	(pseudo)	*FQ2*	$\leq$	45	(min)

Only 20 solutions were found to be feasible according to the above criteria constraints, and all of them are contained in the Pareto optimal set.

Analysis of the histograms shows the effect of the functional and criteria constraints (see Figure 3). The feasible solutions for the design variables *DV1* and *DV2* are located in the middle of the interval, with no feasible solutions in the left and right ends of the intervals, and slightly shifted from the prototype design (marked with a yellow triangle $\bigtriangledown$). These two histograms clearly identify tight intervals for the design variables *DV1* and *DV2* characterizing the state-predictor dynamics. On the other hand, the feasible solutions for the design variables *DV3* and *DV4* are located in the right ends of the intervals. These results will be used in the next step of the optimization process to modify the initial intervals of variation of the design variables to improve the feasible solution set and optimize the prototype design.

It is also important to analyze the influence of the design variables on criteria and pseudocriteria, and to evaluate the degree of improvement (or degradation) of the Pareto optimal solutions with respect to the prototype design. Figures 4 to 8 show some of these dependencies, which are valuable to get insight into the effect of the design variables on the augmented-aircraft dynamics. Preliminary conclusions that can be drawn from this analysis are detailed next:

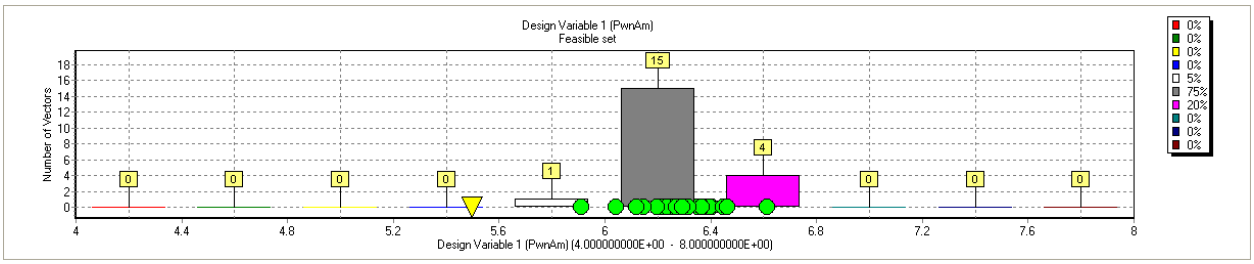

(a) *DV1*

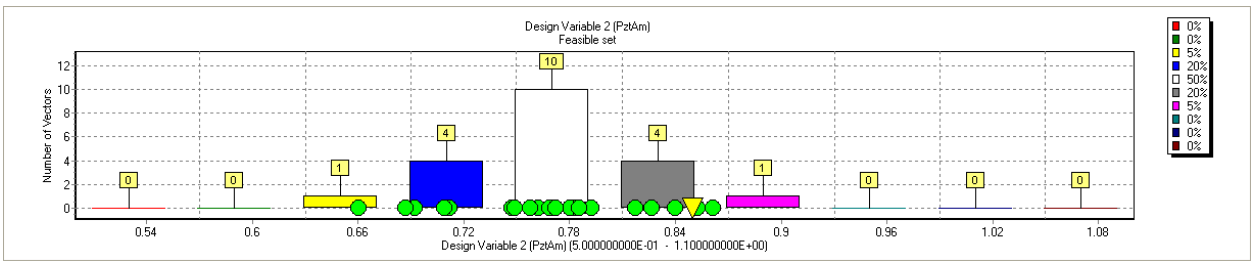

(b) *DV2*

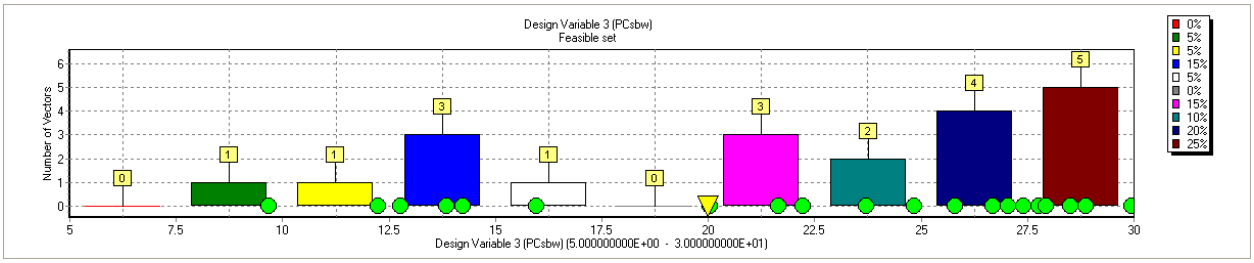

(c) *DV3*

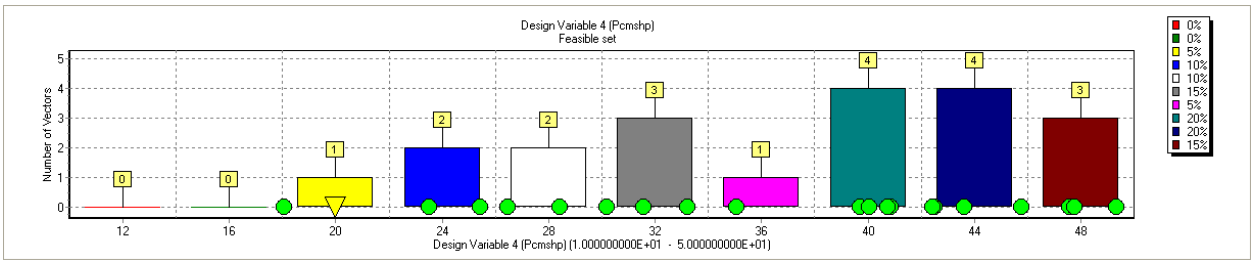

(d) *DV4*

Figure 3: *PSI Iteration 1.* Histograms of the distribution of feasible solutions. The percentage of feasible designs entering the corresponding interval is indicated on the right of the histogram. The Pareto optimal vectors are marked with green circles, while the prototype design is marked with a yellow triangle.

- Figure 4 shows the dependencies of criteria *P2*, *P3*, and *P6* on the design variable *DV1*. First, we notice that there are no feasible solutions in the range $4 < DV1 < 4.6$, which indicates that such design variable vectors did not satisfy the functional constraints. This is consistent with the conclusions drawn from the analysis of the table of functional failures. Second, we also see that the deviations of the actual response of the augmented-aircraft from the desired model become large for big values of the design variable *DV1*. And third, Figures 4a and 4b show that the set of Pareto optimal solutions, when compared to the prototype design, provide step responses with reduced deviations in terms of both (truncated) $\mathcal{L}_\infty$- and $\mathcal{L}_2$-norms. The rate deviations for the Pareto optimal solutions are, however, larger than the rate deviations for the prototype design (see Figure 4c).

- Figure 5 presents the dependencies of the flying qualities criteria *FQ1* and *FQ2* on the design variable *DV1*, which indicate that faster responses of the augmented-aircraft (large *DV1*) result in improved (predicted) flying qualities. This trend is particularly evident in Figure 5b, in which reduced pilot (lead) compensation is limited to large values of the design variable *DV1*. Also, when compared to the prototype design, the set of optimal solutions improve the criterion *FQ1* by a 20 to 50%, and the criterion *FQ2* by a 15 to 30%.

- As expected, a faster response of the augmented-aircraft (large *DV1*) leads to an increase in the control effort (pseudocriteria *P8*), as well as an increase in both the maximum elevator rate and the maximum elevator acceleration (pseudocriteria *P9* and *P10*). Figure 6 illustrates these results.

- Figure 7 shows the dependencies of criteria *FQ1* and *FQ2* on the design variable *DV2*. While the dependency of *FQ2* on *DV2* is not obvious, small values of *DV2* seem to limit the achievable tracking performance with the pilot in the loop (*FQ1*). This would imply that augmented-aircraft with low-damping characteristics result in degraded (predicted) flying qualities.

- Finally, Figure 8 shows the dependencies of pseudocriteria *P9* and *P10* on the design variable *DV4*. We notice that the Pareto optimal solutions are located along a "straight" line, and high values of the criteria correspond to high values of the design variable *DV4*. This implies that the bandwidth of the command prefilter in the $\mathcal{L}_1$ FCS (*DV4*) can be set to limit the maximum elevator rate and the maximum elevator acceleration of the Pareto optimal solutions.

Dependencies between criteria provide useful information about the solutions in the Pareto set and the trade-offs between criteria, which becomes especially helpful in the final stages of the optimization process to make decisions about the most preferable (*optimal*) solution. At this initial stage of the optimization process, however, these dependencies are useful to explore the trade-offs in the design of the controller and to identify directions in the design variable space that may lead to improved $\mathcal{L}_1$ design over the prototype design. Next, we present and discuss a set of graphs showing dependencies between criteria illustrating these trade-offs and determining possible directions of improvement of the prototype solution:

- Figure 9a shows the dependency between *P2* and *P3* (maximum and integral deviations from the desired response) as well as the localization of the Pareto optimal solutions with respect to the prototype design in the *P2*-*P3* plane. This figure provides valuable information about the deviation of the actual response of the augmented-aircraft from the desired response for a given design variable vector. it can be seen that the solutions of the Pareto set are located on a "straight" line passing through the prototype design, and all of them improve the prototype in terms of the metrics *P2* and *P3*.

- Figure 9b shows the location of the prototype as well as the Pareto optimal solutions in the FQ plane of the TDNS criterion, characterizing thus the (predicted) flying qualities of the different solutions. The improvement with respect to the prototype design in terms of predicted FQ is evident in this $FQ2$-$FQ1$ graph. Also, the boundary for level 1 flying qualities of the TDNS criterion can be easily recognized in this figure (see [20]).

- Finally, Figure 9c shows the dependency between the FQ criterion *FQ2* and the control effort *P8*. This figure shows that reduced pilot (lead) compensation is only possible for increased control effort. In fact, all of the solutions in the Pareto set present higher control effort than the prototype solution. It is interesting to note that there are two solutions (#351 and #631) that provide pilot compensation at the level of some of the Pareto optimal solutions with (relatively) smaller control effort. These two

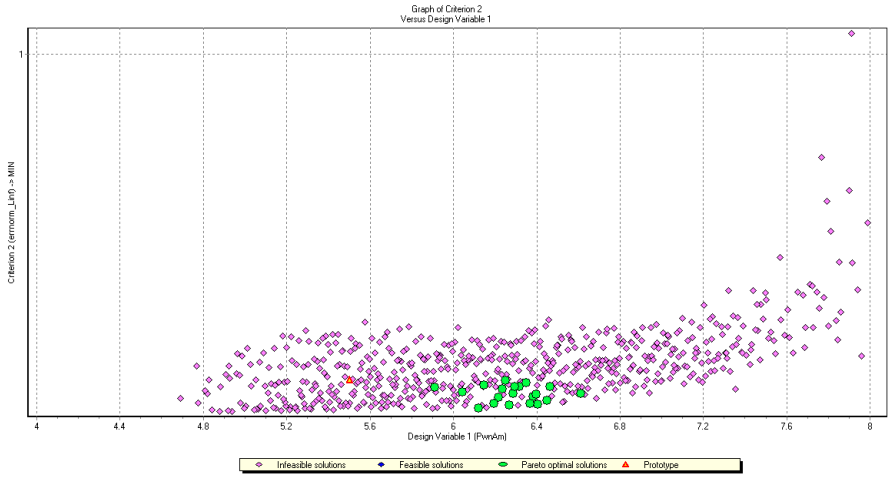

(a) Criterion *P2* vs. design variable *DV1*

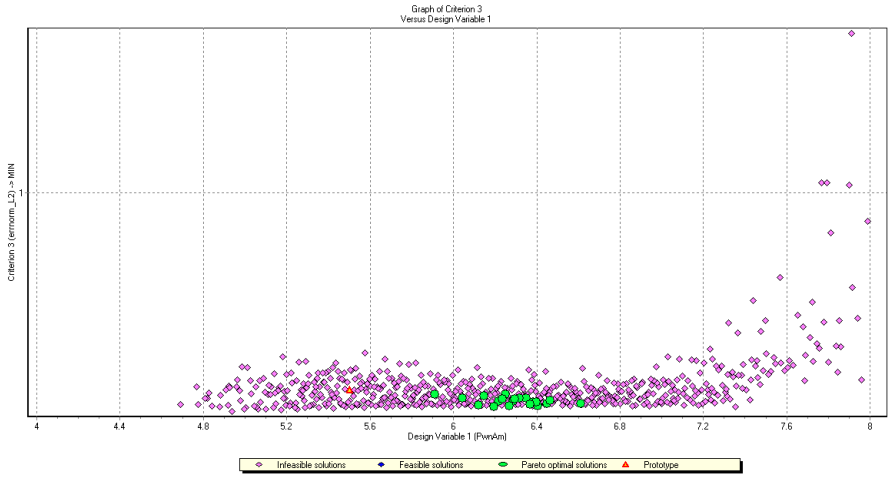

(b) Criterion *P3* vs. design variable *DV1*

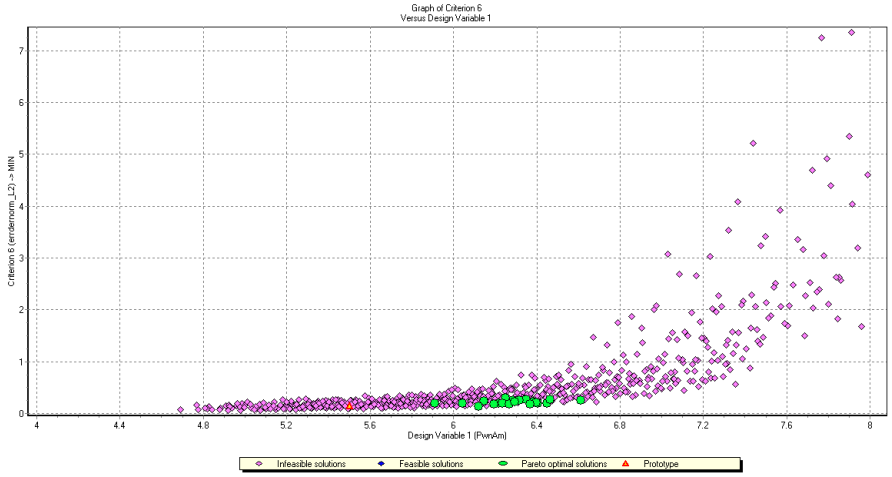

(c) Criterion *P6* vs. design variable *DV1*

Figure 4: *PSI Iteration 1.* Dependencies of criteria *P2*, *P3*, and *P6* on the design variable *DV1*.

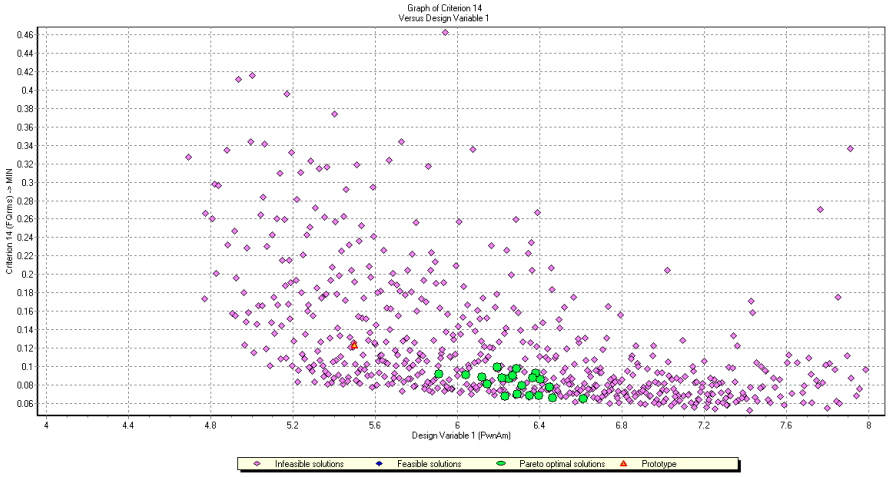

(a) Criterion *FQ1* vs. design variable *DV1*

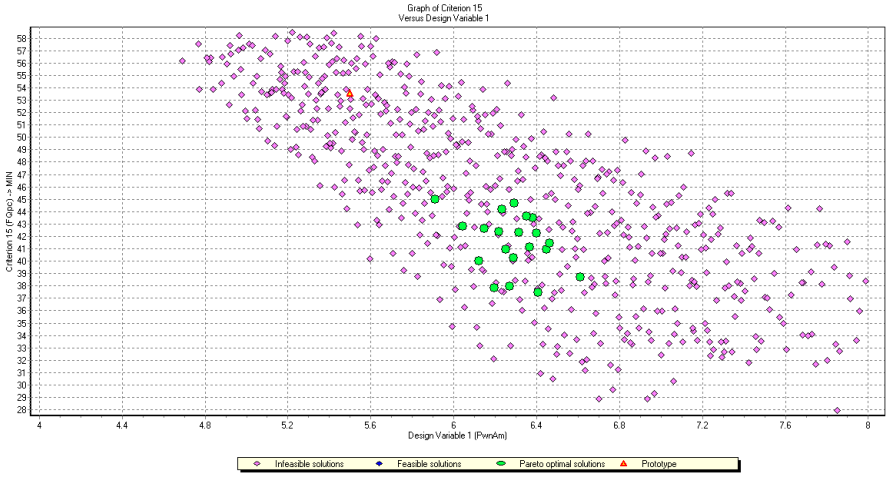

(b) Criterion *FQ2* vs. design variable *DV1*

Figure 5: *PSI Iteration 1.* Dependencies of criteria *FQ1* and *FQ2* on the design variable *DV1*.

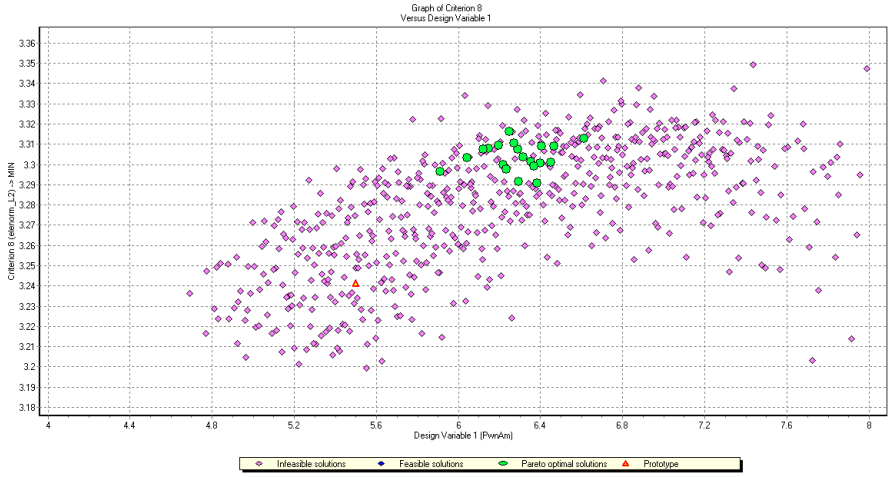

(a) Criterion *P8* vs. design variable *DV1*

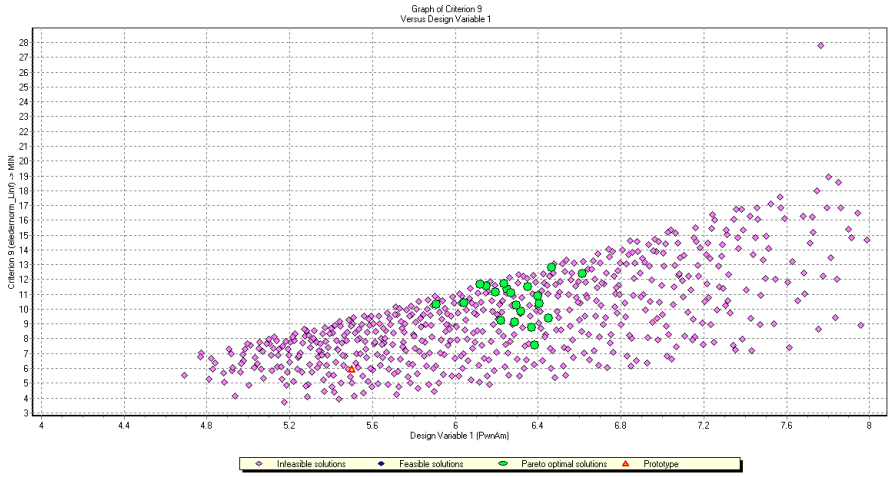

(b) Criterion *P9* vs. design variable *DV1*

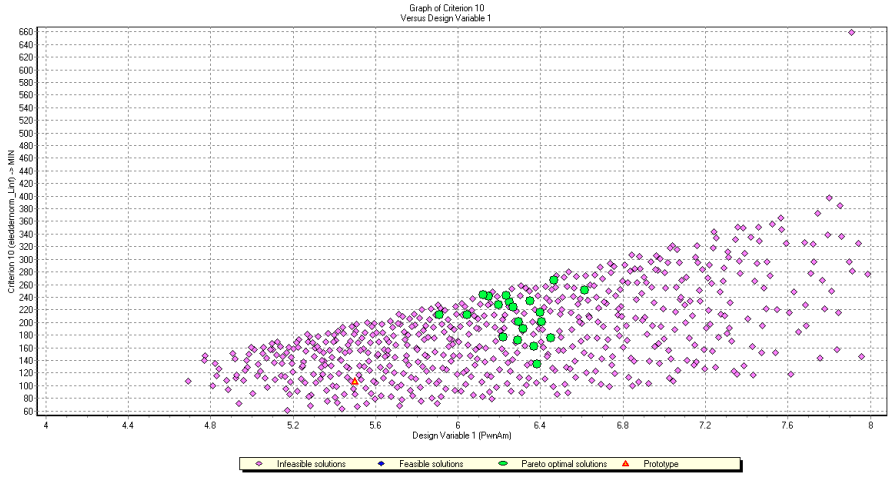

(c) Criterion *P10* vs. design variable *DV1*

Figure 6: *PSI Iteration 1.* Dependencies of criteria *P8*, *P9*, and *P10* on the design variable *DV1*.

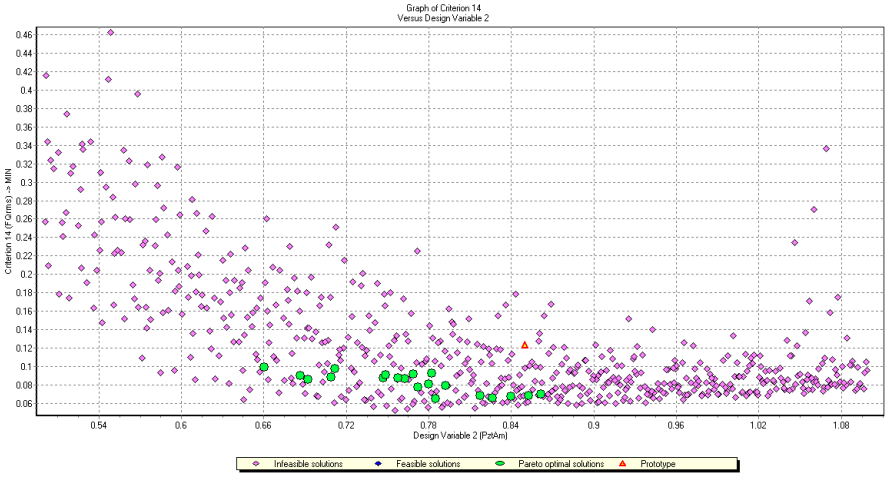

(a) Criterion *FQ1* vs. design variable *DV2*

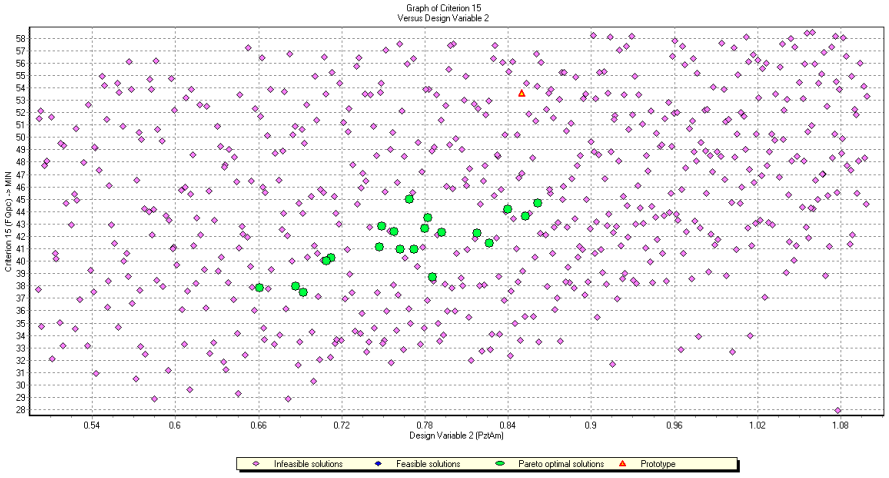

(b) Criterion *FQ2* vs. design variable *DV2*

Figure 7: *PSI Iteration 1.* Dependencies of criteria *FQ1* and *FQ2* on the design variable *DV2*.

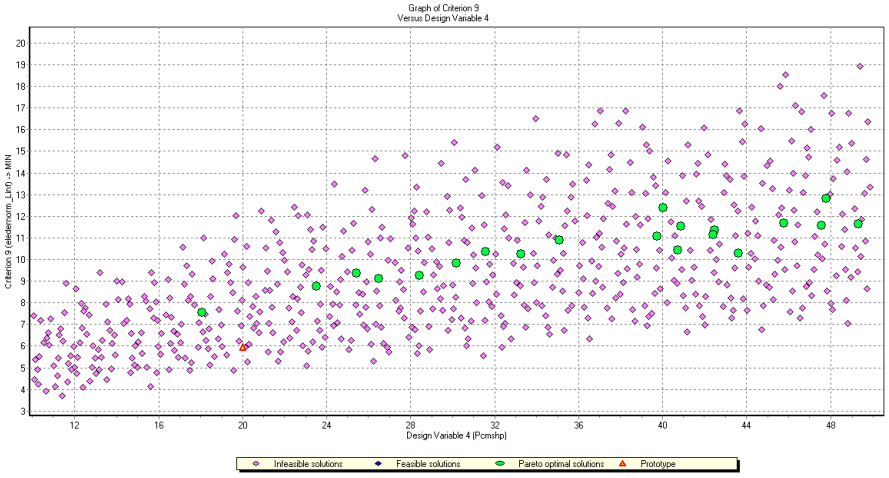

(a) Criterion *P9* vs. design variable *DV4*

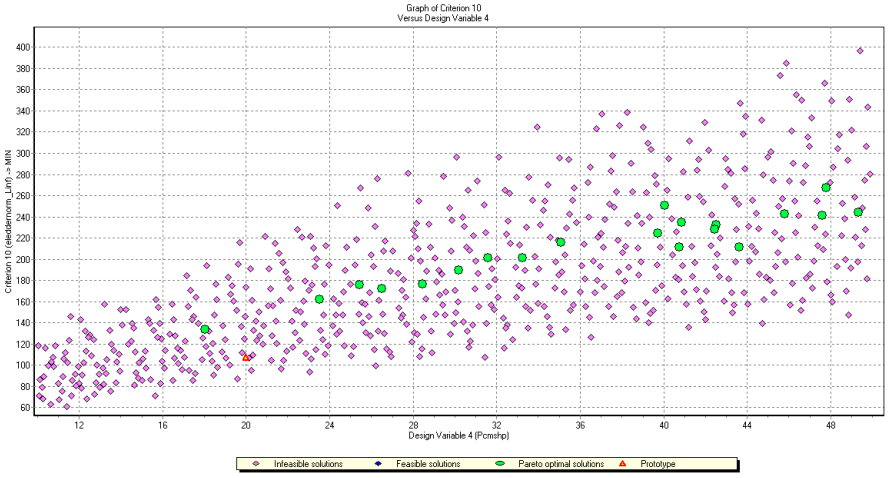

(b) Criterion *P10* vs. design variable *DV4*

Figure 8: *PSI Iteration 1.* Dependencies of criteria *P9* and *P10* on the design variable *DV4*.

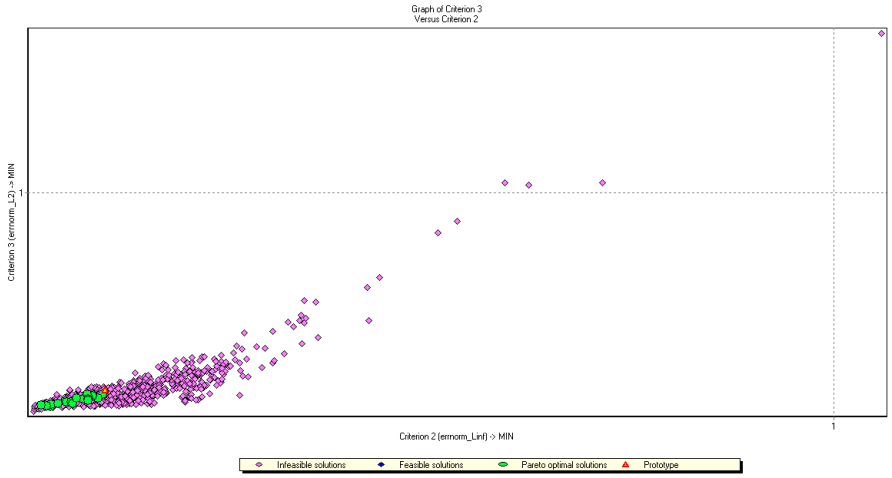

(a) Criterion *P2* vs. criterion *P3*

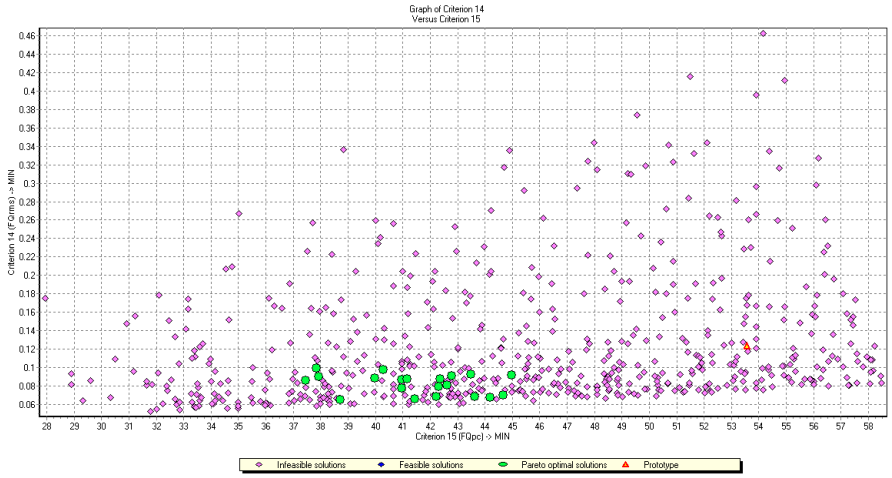

(b) Criterion *FQ1* vs. criterion *FQ2*

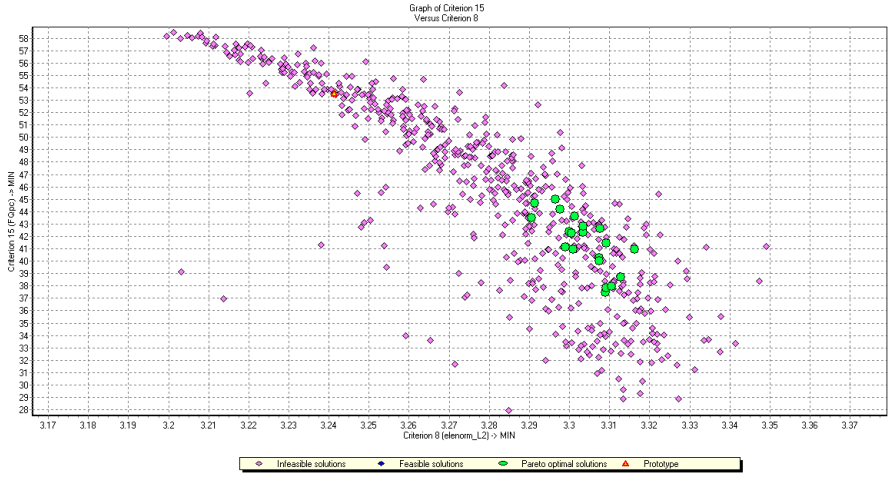

(c) Criterion *FQ2* vs. criterion *P8*

Figure 9: *PSI Iteration 1.* Dependencies between criteria.

Table 3: Refining design variable constraints.

Design variable	Initial intervals of variation of design variables *(Iteration 1)*		Subintervals where the feasible solutions belong *(Iteration 1)*		New Intervals of Variation of design variables *(Iteration 2)*	
	min	max	min	max	min	max
DV1	$4.00{\cdot}10^{0}$	$8.00{\cdot}10^{0}$	$5.70{\cdot}10^{0}$	$6.65{\cdot}10^{1}$	$5.50{\cdot}10^{0}$	$7.00{\cdot}10^{0}$
DV2	$5.00{\cdot}10^{-1}$	$1.10{\cdot}10^{0}$	$6.60{\cdot}10^{-1}$	$8.70{\cdot}10^{-1}$	$6.50{\cdot}10^{-1}$	$9.00{\cdot}10^{-1}$
DV3	$5.00{\cdot}10^{0}$	$3.00{\cdot}10^{1}$	$9.80{\cdot}10^{0}$	$3.00{\cdot}10^{1}$	$9.80{\cdot}10^{0}$	$4.00{\cdot}10^{1}$
DV4	$1.00{\cdot}10^{1}$	$5.00{\cdot}10^{1}$	$1.80{\cdot}10^{1}$	$5.00{\cdot}10^{1}$	$1.80{\cdot}10^{1}$	$6.50{\cdot}10^{1}$

solutions, however, are characterized by large values of the design variables *DV1* and *DV2*, which result in large values of criteria *P2*, *P3*, and *P4*.

This brief analysis of the dependencies between criteria concludes the description of the results obtained in the first step of the optimization process. The set of Pareto optimal solutions obtained in this first experiment clearly determines a direction of improvement in the design variable space. In particular, the results have provided tight intervals for the design variables *DV1* and *DV2* characterizing the state-predictor dynamics, and have exposed the necessity of extending the initial intervals of variation of the design variables *DV3* and *DV4*. Based on these results and the conclusions drawn from them, a new experiment is carried out to (*i*) improve the feasible solution set, and (*ii*) determine an optimal solution to the $\mathcal{L}_1$ FCS design problem that improves the prototype design.

3. Design Improvement

In order to improve the feasible solution set, and based on careful analysis of the histograms in Figure 3, we adjust the initial problem statement by changing the initial intervals of variation of the design variables as follows (see Table 3):

$$\begin{aligned} 5.5 \;&\leq\; DV1 \;\leq\; 7 && \text{(rad/sec)} \\ 0.65 \;&\leq\; DV2 \;\leq\; 0.9 && \\ 9.8 \;&\leq\; DV3 \;\leq\; 40 && \text{(rad/sec)} \\ 18 \;&\leq\; DV4 \;\leq\; 65 && \text{(rad/sec)}\,. \end{aligned}$$

The functional constraints remain unchanged, whereas the design is now to be optimized with respect to the following new set of criteria:

$$P2\,,\quad P3\,,\quad P4\,,\quad P5\,,\quad P6\,,\quad R1\,,\quad FQ1\,,\quad FQ2\,,\quad FQ4\,.$$

All these criteria are to be minimized except for *R1*, which is to be maximized and it is subject to the control specification *S2* ($R1 \geq 80$). Additionally, the following set of metrics is considered as *pseudocriteria*:

$$P7\,,\quad P8\,,\quad P9\,,\quad P10\,,\quad P11\,,\quad P12\,,\quad P13\,.$$

Next we present the results obtained in this second step of the optimization process, which are based on a single iteration using 512 design variable vectors generated with uniformly distributed sequences. We note that the addition of criteria *R1* and *FQ4* in the optimization process represents a significant increase in the computational time.

All of the 512 samples in the design variable space satisfied the "rigid" functional constraints. Initially, the same criteria and pseudocriteria constraints used in the first PSI iteration were kept in this second iteration:

P2	$\leq$	0.2	(min)	*P10*	$\leq$	300	(pseudo)
P3	$\leq$	0.2	(min)	*P11*	$\leq$	0.25	(pseudo)
P4	$\leq$	1.05	(min)	*P12*	$\leq$	0.01	(pseudo)
P5	$\leq$	1	(min)	*P13*	$\leq$	0.01	(pseudo)
P6	$\leq$	0.3	(min)	*FQ1*	$\leq$	0.1	(min)
P7	$\leq$	0.25	(pseudo)	*FQ2*	$\leq$	45	(min)
P8	$\leq$	5	(pseudo)	*FQ4*	$\leq$	–	(min)
P9	$\leq$	15	(pseudo)	*R1*	$\leq$	–	(max)

With these constraints, 124 vectors were found to be feasible, which represents an increase in the coefficient of searching the feasible solution set[d] by more than 12 times. Furthermore, the histograms in this second iteration have better distributions of the feasible solutions than in the first iteration (see Figure 10). As the only purpose of this set of histograms is to show the improvement in the construction of the feasible set, the Pareto optimal solutions are not shown.

Using the same data and after careful analysis of the test table, stronger criteria and pseudocriteria constraints were considered:

P2	$\leq$	0.1	(min)	*P10*	$\leq$	200	(pseudo)
P3	$\leq$	0.15	(min)	*P11*	$\leq$	0.1	(pseudo)
P4	$\leq$	1.02	(min)	*P12*	$\leq$	0.01	(pseudo)
P5	$\leq$	1	(min)	*P13*	$\leq$	0.01	(pseudo)
P6	$\leq$	0.25	(min)	*FQ1*	$\leq$	0.1	(min)
P7	$\leq$	0.2	(pseudo)	*FQ2*	$\leq$	45	(min)
P8	$\leq$	5	(pseudo)	*FQ4*	$\leq$	5	(min)
P9	$\leq$	10	(pseudo)	*R1*	$\leq$	80	(max)

According to these new constraints, only 6 solutions were found to be feasible, and all of them are contained in the Pareto optimal set. The values of design variables and criteria of the Pareto optimal solutions are given in Table 4. The new histograms of distribution of the feasible solutions for these stronger criteria and pseudocriteria constraints are shown in Figure 11. These new histograms clearly identify tight intervals for all of the design variables in which the optimal solutions lie. It is important to mention that, since the first and second iterations use a different set of criteria, the solutions could not be combined in MOVI[e].

We analyze again the dependencies of criteria on design variables. The following observations are of particular interest:

- Figure 12 shows the influence of the bandwidth of the "matched" low-pass filter (design variable *DV3*) on the (pilot-off-the-loop) trade-off between performance (criteria *P2* and *P3*) and robustness (criterion *R1*) of the augmented-aircraft. We can conclude that criteria *P2* (or *P3*) and *R1* are in conflict with each other with respect to the design variable *DV3*. This means that improvement of the tracking performance requires an increase in the bandwidth of the low-pass filter, which in its turn results in a deterioration of the time-delay margin of the augmented-aircraft, as predicted by theory.

- Figure 13 shows the dependencies of the flying qualities criteria *FQ1* and *FQ2* on the design variable *DV2*. While in the first PSI iteration the dependency of the criterion *FQ2* on the design variable *DV2* was not obvious (see Figure 7b), the dependency becomes more apparent from the data obtained in this second iteration; in fact, Figure 13b shows that a smaller damping ratio seems to result in reduced (lead) pilot compensation.

[d]The *coefficient of searching the feasible solution set*, usually denoted by γ_F, is defined as the ratio of feasible solutions to the total number of tests performed.

[e]The combination of feasible solution sets (or optimal Pareto sets) from different experiments is a feature of the MOVI software package that becomes very useful in real-life optimization problems. In particular, the construction of combined sets allows to estimate the contribution of each experiment to the set of feasible (or optimal) solutions, which provides a measure of improvement in the construction of the feasible (or optimal) solution set. The construction of combined solution sets is also useful in problems that require either a large number of samples in the design variable space, or a significant amount of computer time for the computation of every criteria vector.

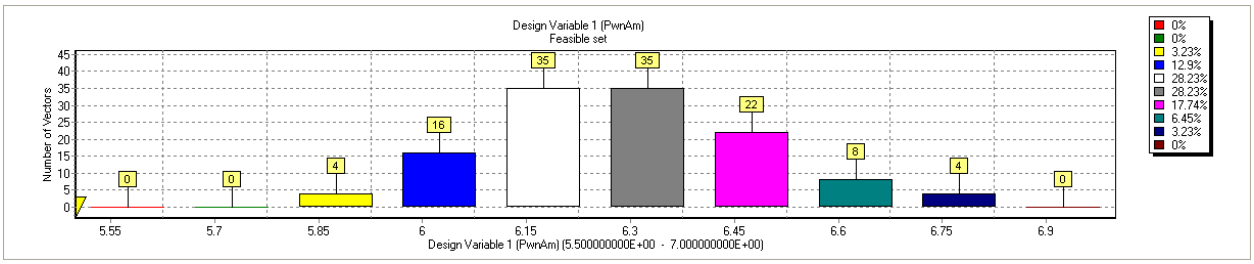

(a) *DV1*

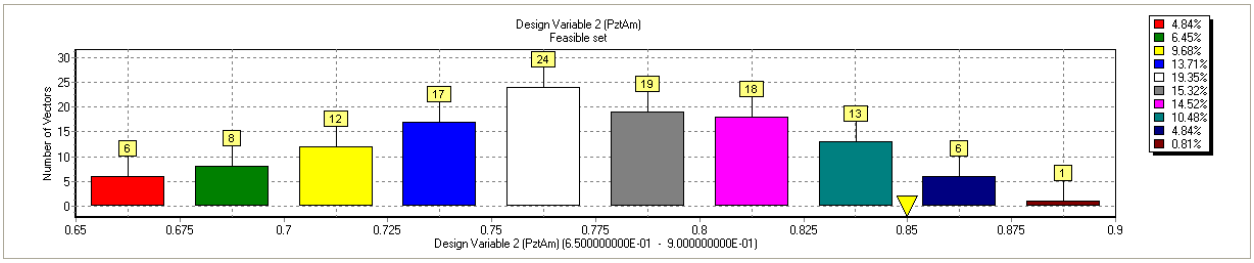

(b) *DV2*

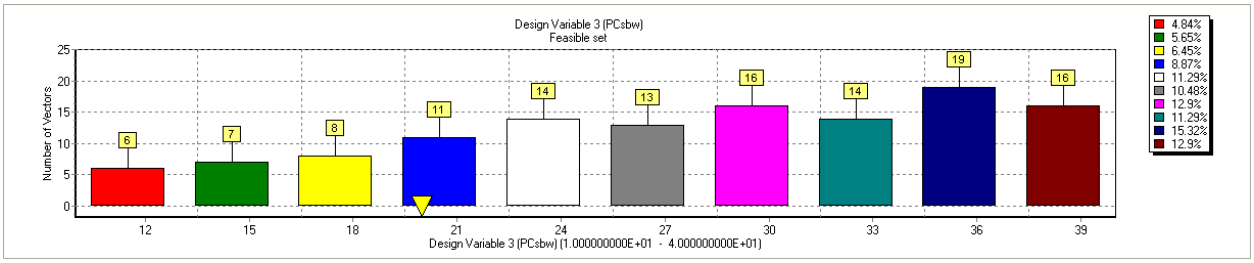

(c) *DV3*

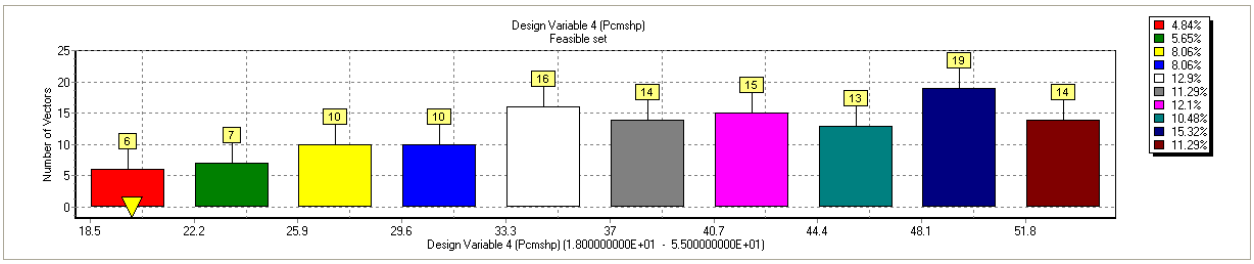

(d) *DV4*

Figure 10: *PSI Iteration 2*. Histograms of the distribution of feasible solutions with the original criteria constraints. The percentage of feasible designs entering the corresponding interval is indicated on the right of the histogram. The prototype design is marked with a yellow triangle.

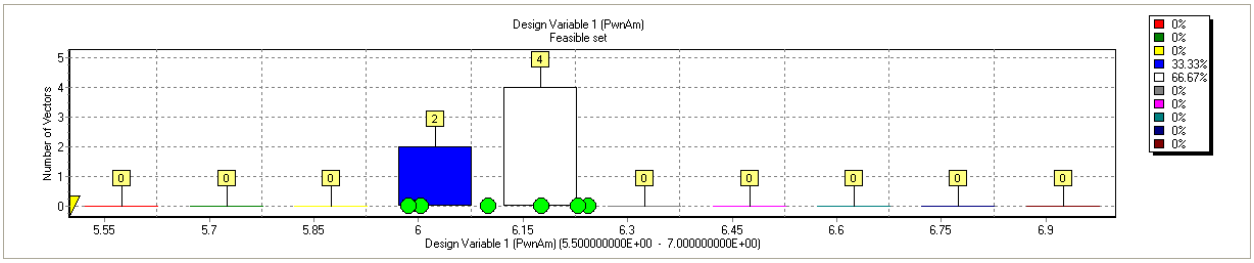

(a) *DV1*

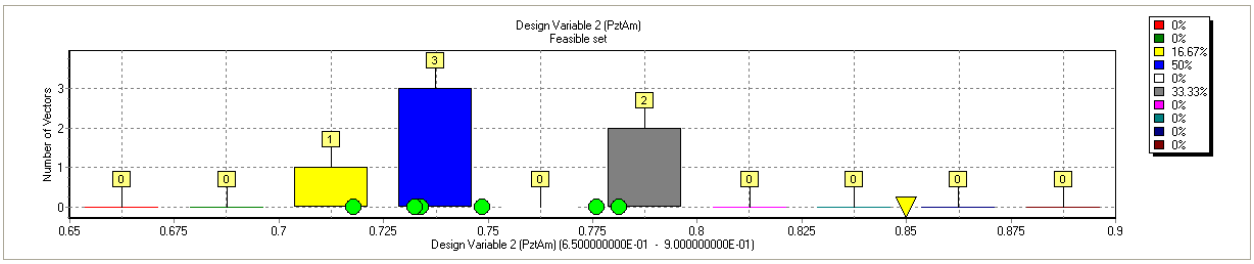

(b) *DV2*

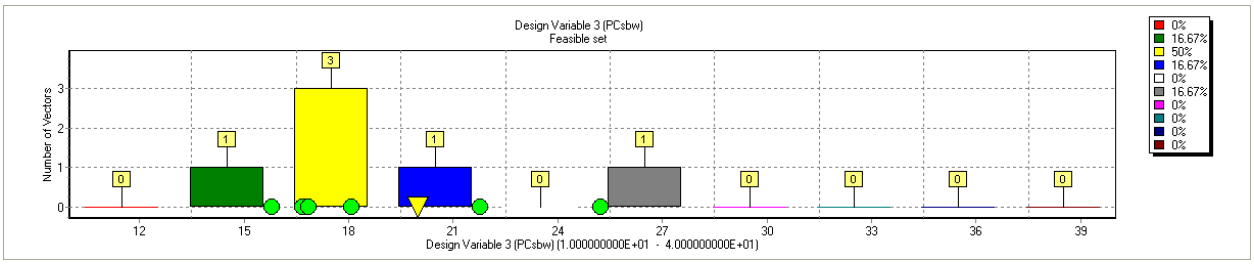

(c) *DV3*

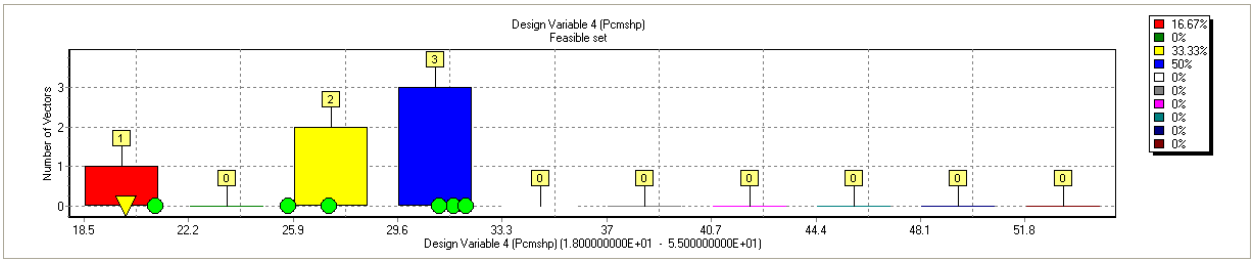

(d) *DV4*

Figure 11: *PSI Iteration 2*. Histograms of the distribution of feasible solutions with the new (stronger) criteria constraints. The percentage of feasible designs entering the corresponding interval is indicated on the right of the histogram. The Pareto optimal vectors are marked with green circles, while the prototype design is marked with a yellow triangle.

Table 4: *PSI Iteration 2*. Pareto optimal solutions.

(a) Table of Design Variables.

Design variable	Prototype	Pareto optimal solutions					
		#106	#202	#254	#318	#358	#462
DV1	$5.50 \cdot 10^{0}$	$6.00 \cdot 10^{0}$	$5.99 \cdot 10^{0}$	$6.24 \cdot 10^{0}$	$6.23 \cdot 10^{0}$	$6.10 \cdot 10^{0}$	$6.18 \cdot 10^{0}$
DV2	$8.50 \cdot 10^{-1}$	$7.34 \cdot 10^{-1}$	$7.49 \cdot 10^{-1}$	$7.76 \cdot 10^{-1}$	$7.33 \cdot 10^{-1}$	$7.81 \cdot 10^{-1}$	$7.18 \cdot 10^{-1}$
DV3	$2.00 \cdot 10^{1}$	$2.52 \cdot 10^{1}$	$1.67 \cdot 10^{1}$	$1.81 \cdot 10^{1}$	$2.18 \cdot 10^{1}$	$1.69 \cdot 10^{1}$	$1.58 \cdot 10^{1}$
DV4	$2.00 \cdot 10^{1}$	$3.16 \cdot 10^{1}$	$3.20 \cdot 10^{1}$	$2.10 \cdot 10^{1}$	$2.72 \cdot 10^{1}$	$2.57 \cdot 10^{1}$	$3.11 \cdot 10^{1}$

(b) Table of Criteria.

Criteria		Prototype	Pareto optimal solutions					
			#106	#202	#254	#318	#358	#462
P2	(min)	$1.30 \cdot 10^{-1}$	$6.01 \cdot 10^{-2}$	$8.45 \cdot 10^{-2}$	$9.17 \cdot 10^{-2}$	$7.04 \cdot 10^{-2}$	$9.63 \cdot 10^{-2}$	$8.28 \cdot 10^{-2}$
P3	(min)	$1.54 \cdot 10^{-1}$	$9.60 \cdot 10^{-2}$	$1.13 \cdot 10^{-1}$	$1.11 \cdot 10^{-1}$	$9.66 \cdot 10^{-2}$	$1.18 \cdot 10^{-1}$	$1.04 \cdot 10^{-1}$
P4	(min)	$1.00 \cdot 10^{0}$	$1.00 \cdot 10^{0}$	$1.00 \cdot 10^{0}$	$1.00 \cdot 10^{0}$	$1.00 \cdot 10^{0}$	$1.00 \cdot 10^{0}$	$1.00 \cdot 10^{0}$
P5	(min)	$3.15 \cdot 10^{-1}$	$6.13 \cdot 10^{-1}$	$6.81 \cdot 10^{-1}$	$8.85 \cdot 10^{-1}$	$8.43 \cdot 10^{-1}$	$7.71 \cdot 10^{-1}$	$8.63 \cdot 10^{-1}$
P6	(min)	$1.49 \cdot 10^{-1}$	$1.28 \cdot 10^{-1}$	$1.67 \cdot 10^{-1}$	$2.16 \cdot 10^{-1}$	$1.78 \cdot 10^{-1}$	$1.94 \cdot 10^{-1}$	$2.11 \cdot 10^{-1}$
P7	(pseudo)	$1.51 \cdot 10^{-1}$	$1.68 \cdot 10^{-1}$	$1.67 \cdot 10^{-1}$	$1.72 \cdot 10^{-1}$	$1.76 \cdot 10^{-1}$	$1.68 \cdot 10^{-1}$	$1.78 \cdot 10^{-1}$
P8	(pseudo)	$3.24 \cdot 10^{0}$	$3.29 \cdot 10^{0}$	$3.29 \cdot 10^{0}$	$3.29 \cdot 10^{0}$	$3.30 \cdot 10^{0}$	$3.29 \cdot 10^{0}$	$3.31 \cdot 10^{0}$
P9	(pseudo)	$5.96 \cdot 10^{0}$	$9.09 \cdot 10^{0}$	$9.10 \cdot 10^{0}$	$7.90 \cdot 10^{0}$	$9.05 \cdot 10^{0}$	$8.43 \cdot 10^{0}$	$9.54 \cdot 10^{0}$
P10	(pseudo)	$1.07 \cdot 10^{2}$	$1.77 \cdot 10^{2}$	$1.78 \cdot 10^{2}$	$1.43 \cdot 10^{2}$	$1.72 \cdot 10^{2}$	$1.59 \cdot 10^{2}$	$1.85 \cdot 10^{2}$
P11	(pseudo)	$7.45 \cdot 10^{-2}$	$6.62 \cdot 10^{-2}$	$6.60 \cdot 10^{-2}$	$6.09 \cdot 10^{-2}$	$6.74 \cdot 10^{-2}$	$6.31 \cdot 10^{-2}$	$6.95 \cdot 10^{-2}$
P12	(pseudo)	$1.01 \cdot 10^{-4}$	$1.81 \cdot 10^{-4}$	$1.70 \cdot 10^{-4}$	$1.80 \cdot 10^{-4}$	$2.01 \cdot 10^{-4}$	$1.69 \cdot 10^{-4}$	$1.98 \cdot 10^{-4}$
P13	(pseudo)	$3.16 \cdot 10^{-5}$	$6.02 \cdot 10^{-5}$	$5.89 \cdot 10^{-5}$	$6.58 \cdot 10^{-5}$	$7.13 \cdot 10^{-5}$	$6.01 \cdot 10^{-5}$	$7.27 \cdot 10^{-5}$
FQ1	(min)	$1.23 \cdot 10^{-1}$	$9.93 \cdot 10^{-2}$	$9.81 \cdot 10^{-2}$	$9.34 \cdot 10^{-2}$	$9.26 \cdot 10^{-2}$	$9.20 \cdot 10^{-2}$	$9.64 \cdot 10^{-2}$
FQ2	(min)	$5.36 \cdot 10^{1}$	$4.33 \cdot 10^{1}$	$4.41 \cdot 10^{1}$	$4.38 \cdot 10^{1}$	$4.14 \cdot 10^{1}$	$4.46 \cdot 10^{1}$	$4.10 \cdot 10^{1}$
FQ4	(min)	$4.68 \cdot 10^{0}$	$4.08 \cdot 10^{0}$	$4.19 \cdot 10^{0}$	$3.87 \cdot 10^{0}$	$3.88 \cdot 10^{0}$	$3.84 \cdot 10^{0}$	$3.97 \cdot 10^{0}$
R1	(max)	$8.50 \cdot 10^{1}$	$8.50 \cdot 10^{1}$	$1.05 \cdot 10^{2}$	$8.00 \cdot 10^{1}$	$8.50 \cdot 10^{1}$	$9.00 \cdot 10^{1}$	$1.10 \cdot 10^{2}$

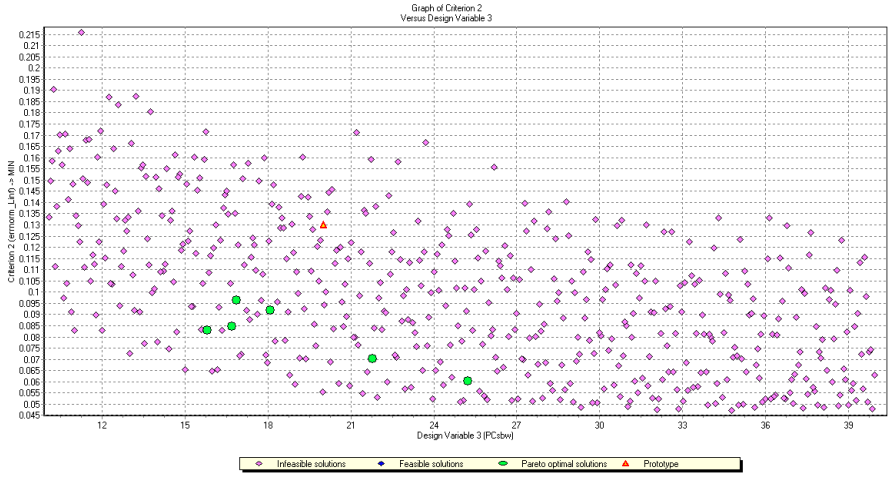

(a) Criterion *P2* vs. design variable *DV3*

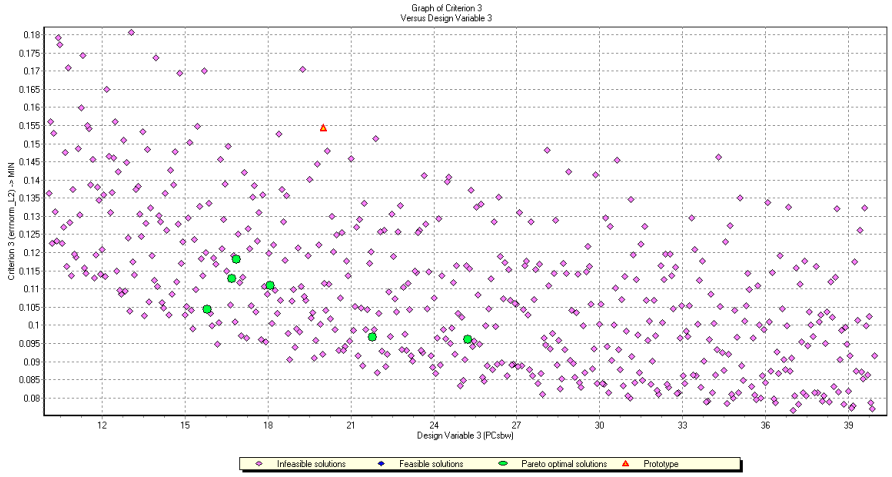

(b) Criterion *P3* vs. design variable *DV3*

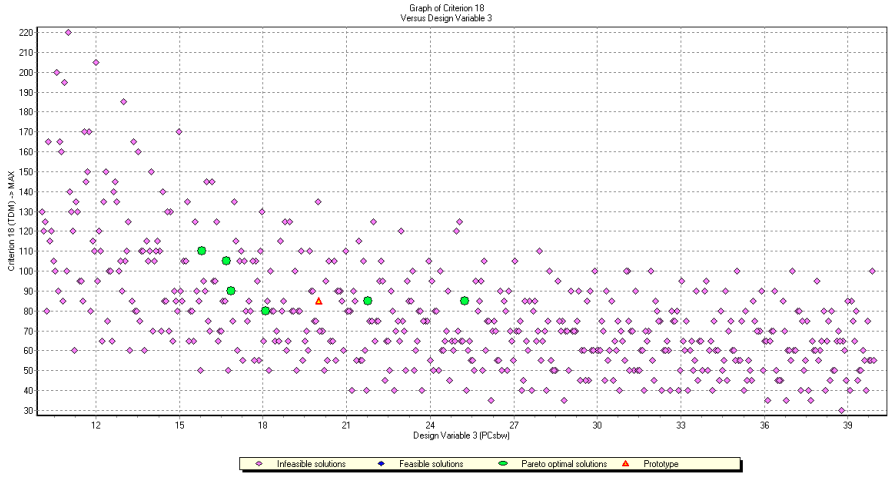

(c) Criterion *R1* vs. design variable *DV3*

Figure 12: *PSI Iteration 2*. Dependencies of criteria *P2*, *P3*, and *R1* on the design variable *DV3*.

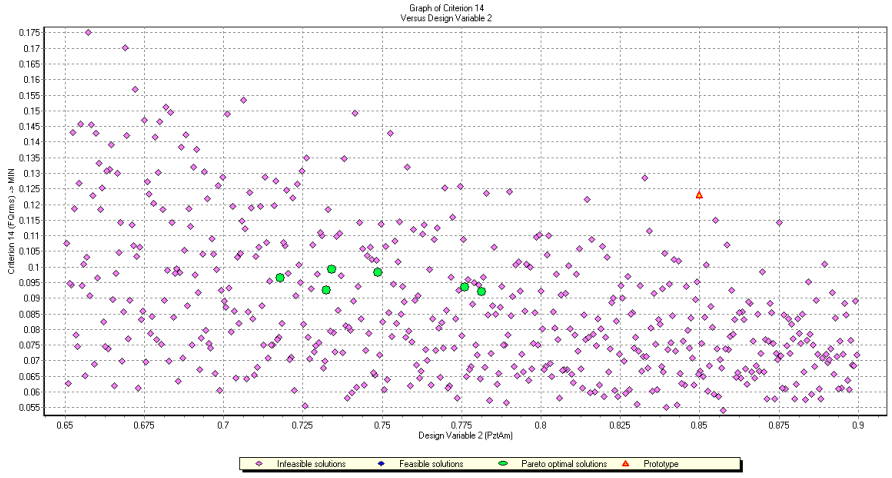

(a) Criterion *FQ1* vs. design variable *DV2*

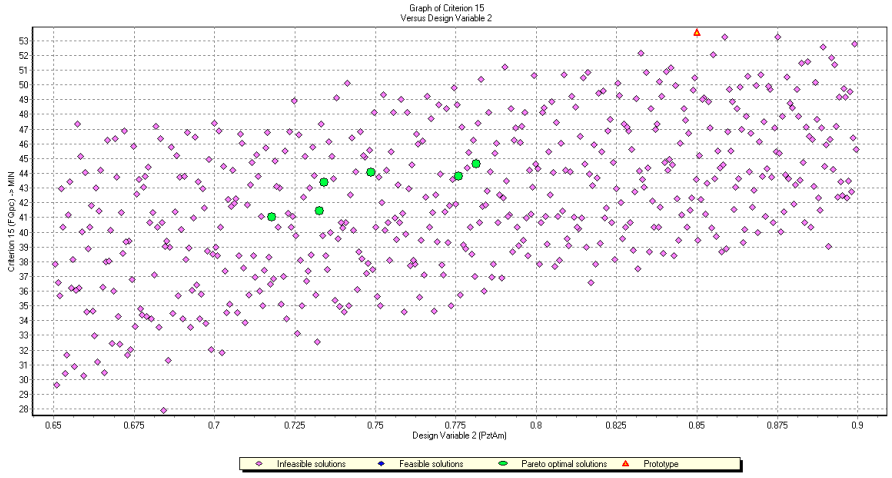

(b) Criterion *FQ2* vs. design variable *DV2*

Figure 13: *PSI Iteration 2*. Dependencies of criteria *FQ1* and *FQ2* on the design variable *DV2*.

Figure 14 shows dependencies between criteria that are relevant to make decisions about the final (most preferable) design of the $\mathcal{L}_1$ FCS:

- Similar to Figure 9a, Figure 14a shows the dependency between *P2* and *P3*. All of the Pareto optimal solutions improve the prototype design in terms of peak and integral deviations from the desired response.
- The FQ parameter plane of the TDNS criterion is shown in Figure 14b, which reveals a considerable improvement in terms of predicted flying qualities of the Pareto optimal solutions over the prototype design.
- Finally, Figure 14c shows the dependency between criteria *P3* and *R1*, which illustrates the trade-off between performance and robustness of the closed-loop adaptive system with the pilot off the loop. While all of the optimal solutions reduce the deviations from the desired response with respect to the prototype design (as already shown in Figure 14a), only three of these solutions exhibit a better time-delay margin than the prototype design (#202, #462), and two exhibit a similar margin (#106, #318)[f].

After careful analysis of the criteria in Table 4b and the criteria dependencies in Figure 14, the preference is given to the vector #202. This vector provides a good trade-off between (predicted) flying qualities and time-delay margin, and it improves the prototype design in six criteria.

4. Sensitivity Analysis of the Optimal Solution

Finally, in this section we conduct an analysis of the sensitivity of the criteria to the design variables in the vicinity of the optimal solution chosen in the previous section (vector #202). As explained earlier, this last step in the design optimization process is important to ensure robustness of this *optimal* solution to small variations of the design variables. The sensitivity analysis is based on a systematic directional search in the design variable space with the objective of exploring the susceptibility of criteria to (small) changes in design variables.

To illustrate this final step, Figures 15 and 16 show the dependencies of flying qualities, robustness, and desired-model tracking performance criteria on the design variables *DV1* and *DV3* for the vector #202 (for each plot, only one design variable is changing while all the remaining design variables are fixed at the optimal value). In particular, Figure 15 shows that the flying qualities criteria (*FQ1* and *FQ2*) and the time-delay margin of the augmented-aircraft (*R1*) are in conflict with each other with respect to the natural frequency of the state-predictor eigenvalues (*DV1*). Similarly, Figure 16 shows that the (integral) deviation of the augmented-aircraft response from the desired model (*P3*) and the time-delay margin of the augmented-aircraft (*R1*) are also in conflict with each other with respect to the bandwidth of the low-pass filter in the matched channel of the $\mathcal{L}_1$ FCS (*DV3*), which is in agreement with the theory. Similar contradicting dependencies can be found for the damping ratio of the state-predictor eigenvalues and the bandwidth of the prefilter (design variables *DV2* and *DV4* respectively), which prove the stability of the vector #202.

These results confirm that the design vector #202 provides a good trade-off between (predicted) flying qualities and time-delay margin, while minimizing the distance to the desired response (see Figure 17).

IV. Conclusions

This paper presented preliminary results of the application of the PSI method and the MOVI software package for the design optimization of the $\mathcal{L}_1$ flight control system implemented on the GTM AirSTAR aircraft. In particular, the study has addressed the construction of the feasible solution set, the improvement of a nominal *prototype* design, and the sensitivity analysis of the most preferable (*optimal*) solution. On the one hand, the paper has demonstrated that the consistent application of the systematic design guidelines of $\mathcal{L}_1$ adaptive control becomes particularly beneficial for the *construction of the feasible solution set*, by

[f]Notice that for the determination of the time-delay margin, metric *R1*, we insert incremental time delays of 5 msec in the elevator command channel. This choice was made for consistency with the determination of the time-delay margin in the AirSTAR real-time simulator at NASA LaRC. As a consequence, however, we cannot identify the time-delay margin with higher accuracy.

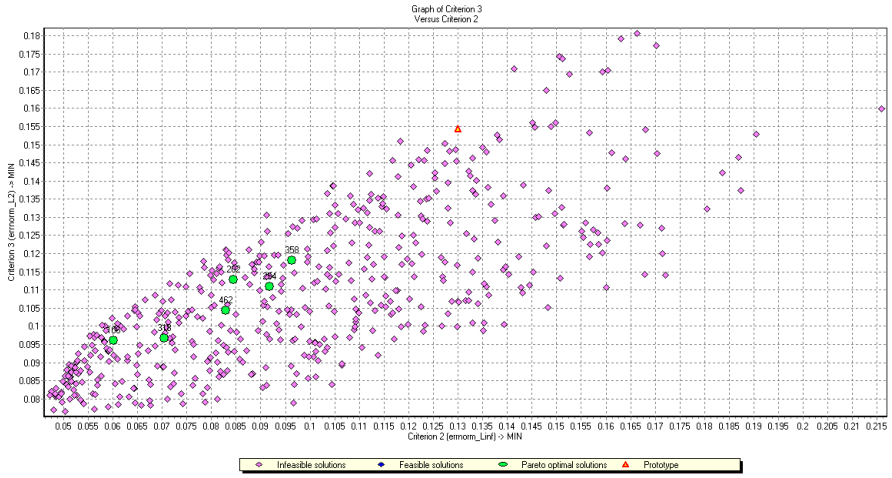

(a) Criterion *P2* vs. criterion *P3*

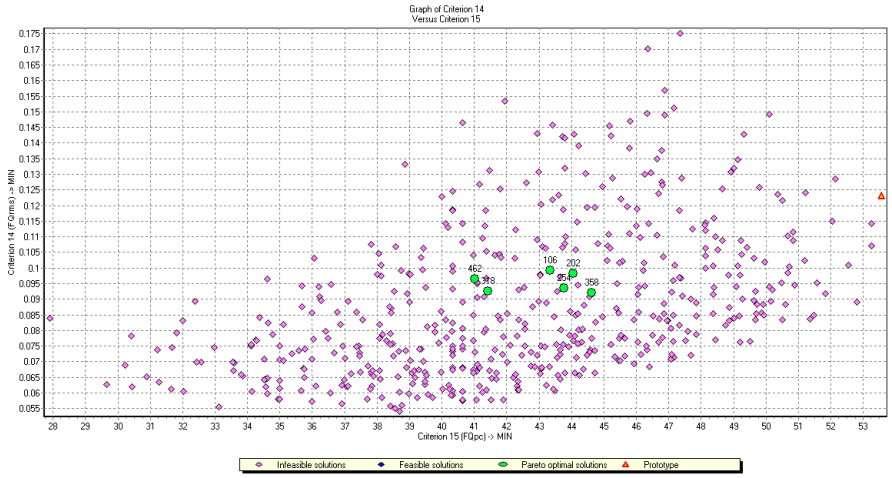

(b) Criterion *FQ1* vs. criterion *FQ2*

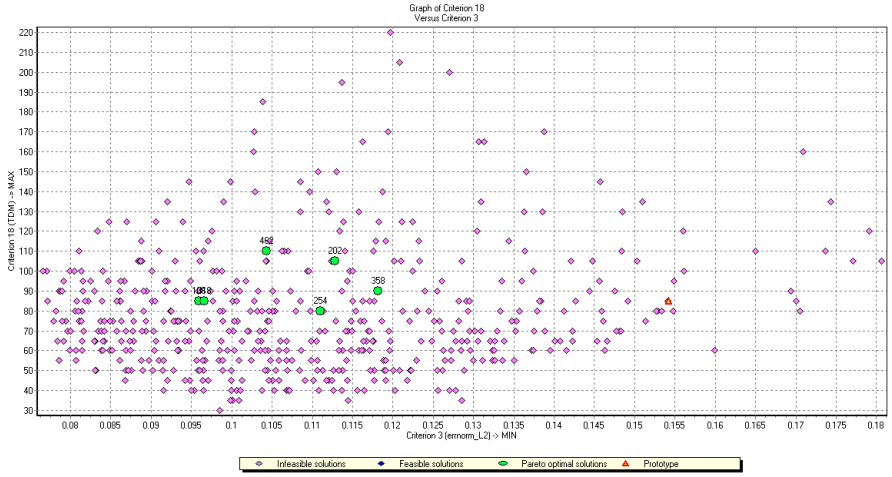

(c) Criterion *R1* vs. criterion *P8*

Figure 14: *PSI Iteration 2*. Dependencies between criteria.

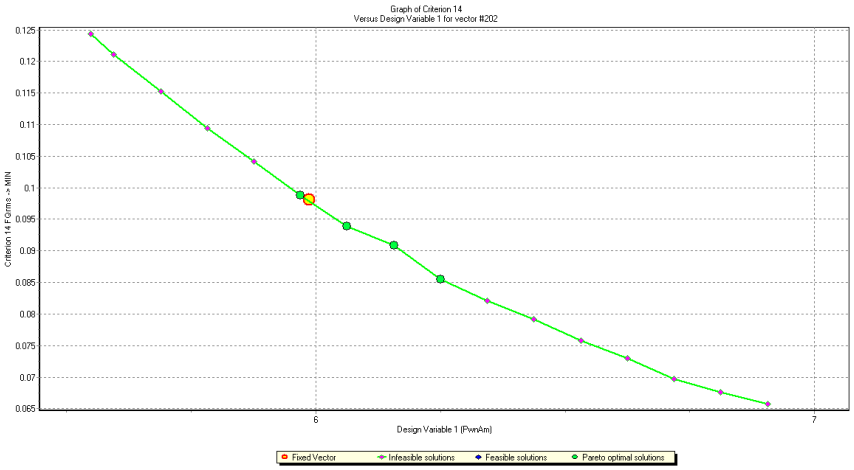

(a) Criterion *FQ1* vs. design variable *DV1*

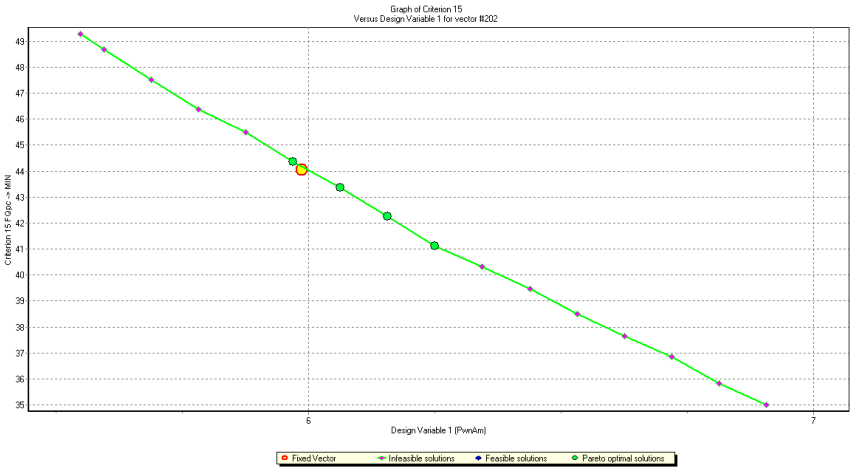

(b) Criterion *FQ2* vs. design variable *DV1*

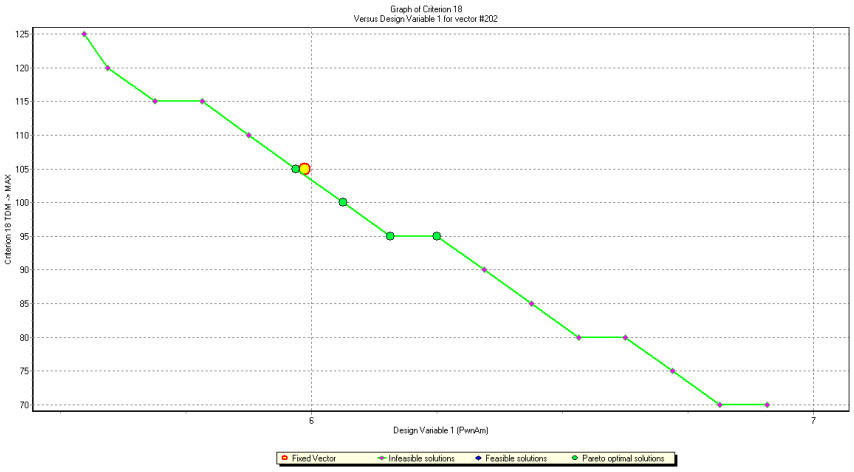

(c) Criterion *R1* vs. design variable *DV1*

Figure 15: Dependency of criteria *FQ1*, *FQ2*, and *R1* on the design variable *DV1* for the Pareto optimal solution #202.

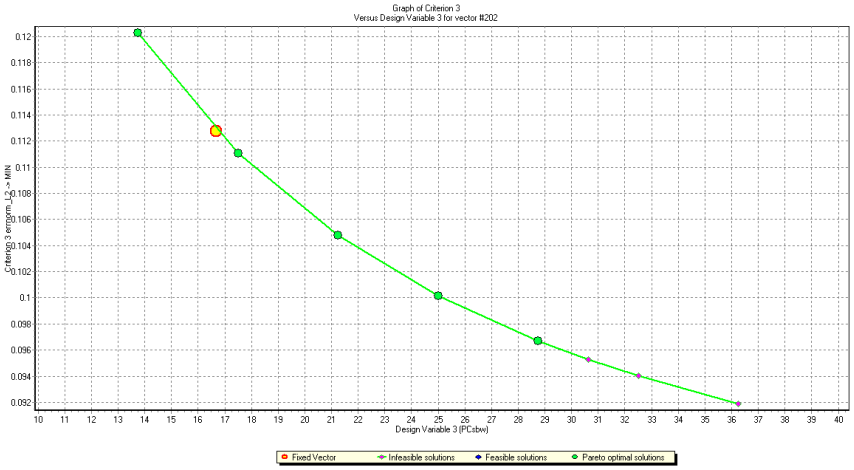

(a) Criterion *P3* vs. design variable *DV3*

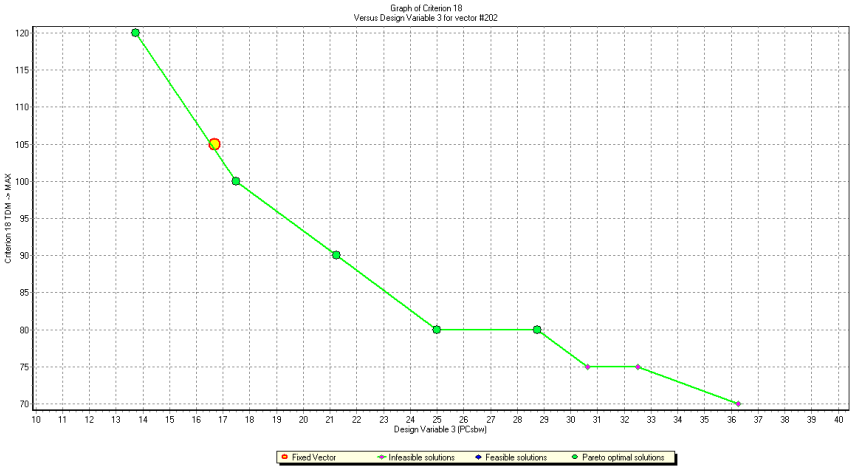

(b) Criterion *R1* vs. design variable *DV3*

Figure 16: Dependency of criteria *P3* and *R1* on the design variable *DV3* for the Pareto optimal solution #202.

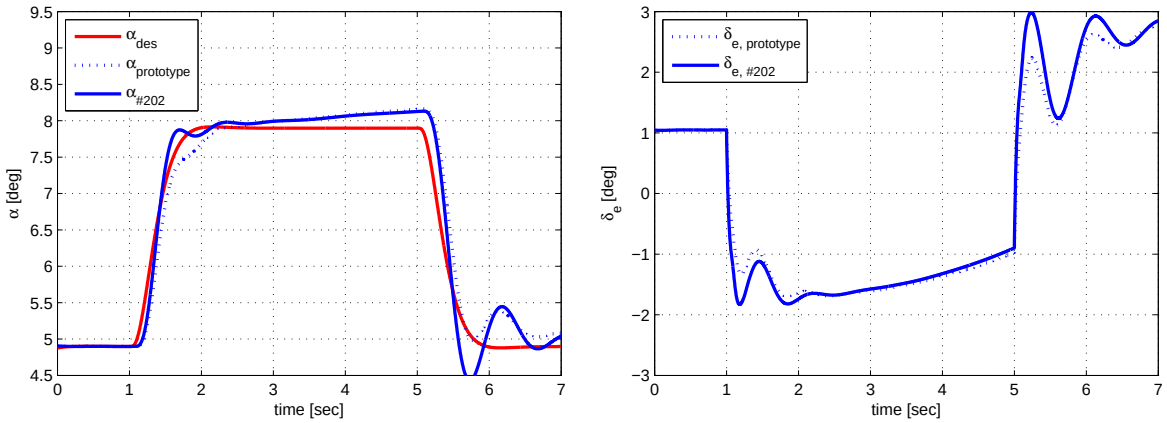

(a) Angle of attack, α

(b) Elevator deflection, δ_e

Figure 17: *Most Preferable Design.* 3 deg-AOA step response for the optimal design #202.

reducing the number of Monte-Carlo sampling trials required for the construction of this set. Moreover, the results of this study are consistent with the theoretical claims of the theory of $\mathcal{L}_1$ Adaptive Control in terms of robustness and performance. On the other hand, the paper confirmed the suitability of the PSI method and the MOVI software package for the multiobjective design optimization of a flight control system subject to desired control specifications. The results of this paper have contributed to the improvement of the (predicted) flying qualities and the robustness margins of the $\mathcal{L}_1$-augmented GTM aircraft.

Acknowledgments

This work was sponsored by Air Force Office of Scientific Research under Contract No. FA9550–09–1–0265 and NASA under Contracts NNX08BA64A and NNX08BA65A.

References

[1]Jacklin, S. A., Lowry, M. R., Schumann, J. M., Gupta, P. P., Bosworth, J. T., Zavala, E., Kelly, J. W., Hayhurst, K. J., Belcastro, C. M., and Belcastro, C. M., "Verification, Validation, and Certification Challenges for Adaptive Flight-Critical Control System Software," *AIAA Guidance, Navigation and Control Conference*, Providence, RI, August 2004, AIAA-2004-5258.

[2]Wise, K. A., Lavretsky, E., and Hovakimyan, N., "Adaptive Control in Flight: Theory, Application, and Open Problems," *American Control Conference*, Minneapolis, MN, June 2006, pp. 5966–5971.

[3]Jacklin, S. A., "Closing Certification Gaps in Adaptive Flight Control Software," *AIAA Guidance, Navigation and Control Conference*, Honolulu, HI, August 2008, AIAA-2008-6988.

[4]Hovakimyan, N. and Cao, C., $\mathcal{L}_1$ *Adaptive Control Theory*, Society for Industrial and Applied Mathematics, Philadelphia, PA, 2010.

[5]Jordan, T. L., Langford, W. M., and Hill, J. S., "Airborne Subscale Transport Aircraft Research Testbed-Aircraft Model Development," *AIAA Guidance, Navigation and Control Conference*, San Francisco, CA, August 2005, AIAA-2005-6432.

[6]Jordan, T. L., Foster, J. V., Bailey, R. M., and Belcastro, C. M., "AirSTAR: A UAV Platform for Flight Dynamics and Control System Testing," *AIAA Aerodynamic Measurement Technology and Ground Testing Conference*, San Francisco, CA, June 2006, AIAA-2006-3307.

[7]Statnikov, R. B. and Matusov, J. B., *Multicriteria Analysis in Engineering: Using the PSI Method with MOVI 1.0*, Kluwer Academic Pub., 2002.

[8]Yanushkevich, I. V., Statnikov, R. B., Statnikov, A. R., and Matusov, J. B., *MOVI 1.3. Software Package*, 2003, `http://www.psi-movi.com`.

[9]Sobol, I. M., "On the Systematic Search in a Hypercube," *SIAM Journal on Numerical Analysis*, Vol. 16, No. 5, 1979, pp. 790–793.

[10]Stadler, W. and Dauer, J., "Multicriteria Optimization in Engineering: A tutorial and Survey," *Structural Optimization: Status and Promise*, 1993, pp. 209–249.

[11]Halton, J., "On the efficiency of certain quasi-random sequences of points in evaluating multi-dimensional integrals," *Numerische Mathematik*, Vol. 2, No. 1, 1960, pp. 84–90.

[12]Hammersley, J., "Monte Carlo methods for solving multivariable problems," *Annals of the New York Academy of Sciences*, Vol. 86, No. Numerical Properties of Functions of More Than One Independent Variable, 1960, pp. 844–874.

[13]Hlawka, E., Schoissengeier, J., Taschner, R., and Thomas, C., *Geometric and analytic number theory*, Springer Berlin, 1991.

[14]Kuipers, L. and Niederreiter, H., *Uniform distribution of sequences*, Wiley New York, 1974.

[15]Xargay, E., Hovakimyan, N., and Cao, C., "$\mathcal{L}_1$ Adaptive Controller for Multi-Input Multi-Output Systems in the Presence of Nonlinear Unmatched Uncertainties," *American Control Conference*, Baltimore, MD, June–July 2010.

[16]Gregory, I. M., Cao, C., Xargay, E., Hovakimyan, N., and Zou, X., "$\mathcal{L}_1$ Adaptive Control Design for NASA AirSTAR Flight Test Vehicle," *AIAA Guidance, Navigation and Control Conference*, Chicago, IL, August 2009, AIAA-2009-5738.

[17]Gregory, I. M., Xargay, E., Cao, C., and Hovakimyan, N., "Flight Test of an $\mathcal{L}_1$ Adaptive Controller on the NASA AirSTAR Flight Test Vehicle," *AIAA Guidance, Navigation and Control Conference*, Toronto, Canada, August 2010.

[18]Kim, K. K. K. and Hovakimyan, N., "Development of Verification and Validation Approaches for $\mathcal{L}_1$ Adaptive Control: Multi-Criteria Optimization for Filter Design," *AIAA Guidance, Navigation and Control Conference*, Toronto, Canada, August 2010.

[19]Stepanyan, V., Krishnakumar, K., Nguyen, N., and Eykeren, L. V., "Stability and performance Metrics for Adaptive Flight Control," *AIAA Guidance, Navigation and Control Conference*, Chicago, IL, August 2009, AIAA-2009-5965.

[20]Bailey, R. E. and Bidlack, T. J., "Unified Pilot-Induced Oscillation Theory. Volume IV: Time-Domain Neal-Smith Criterion," Tech. Rep. WL-TR-96-3031, Air Force Wright Laboratory, December 1995.

[21]Choe, R., Xargay, E., Hovakimyan, N., Cao, C., and Gregory, I. M., "$\mathcal{L}_1$ Adaptive Control under Anomaly: Flying Qualities and Adverse Pilot Interaction," *AIAA Guidance, Navigation and Control Conference*, Toronto, Canada, August 2010.